Molecular Psychiatry (2015) 20, 1350–1365

www.nature.com/mp

ORIGINAL ARTICLE

Modeling non-syndromic autism and the impact of *TRPC6* disruption in human neurons

K Griesi-Oliveira[1,2,12], A Acab[1,12], AR Gupta[3], DY Sunaga[2], T Chailangkarn[1], X Nicol[4], Y Nunez[1], MF Walker[5], JD Murdoch[5], SJ Sanders[5], TV Fernandez[5], W Ji[6], RP Lifton[6], E Vadasz[7], A Dietrich[8], D Pradhan[9], H Song[9], G-l Ming[9], X Gu[10], G Haddad[10], MCN Marchetto[11], N Spitzer[4], MR Passos-Bueno[2], MW State[5] and AR Muotri[1]

An increasing number of genetic variants have been implicated in autism spectrum disorders (ASDs), and the functional study of such variants will be critical for the elucidation of autism pathophysiology. Here, we report a *de novo* balanced translocation disruption of *TRPC6,* a cation channel, in a non-syndromic autistic individual. Using multiple models, such as dental pulp cells, induced pluripotent stem cell (iPSC)-derived neuronal cells and mouse models, we demonstrate that *TRPC6* reduction or haploinsufficiency leads to altered neuronal development, morphology and function. The observed neuronal phenotypes could then be rescued by *TRPC6* complementation and by treatment with insulin-like growth factor-1 or hyperforin, a TRPC6-specific agonist, suggesting that ASD individuals with alterations in this pathway may benefit from these drugs. We also demonstrate that methyl CpG binding protein-2 (MeCP2) levels affect *TRPC6* expression. Mutations in *MeCP2* cause Rett syndrome, revealing common pathways among ASDs. Genetic sequencing of *TRPC6* in 1041 ASD individuals and 2872 controls revealed significantly more nonsynonymous mutations in the ASD population, and identified loss-of-function mutations with incomplete penetrance in two patients. Taken together, these findings suggest that *TRPC6* is a novel predisposing gene for ASD that may act in a multiple-hit model. This is the first study to use iPSC-derived human neurons to model non-syndromic ASD and illustrate the potential of modeling genetically complex sporadic diseases using such cells.

Molecular Psychiatry (2015) **20,** 1350–1365; doi:10.1038/mp.2014.141; published online 11 November 2014

INTRODUCTION

Autism spectrum disorders (ASDs) are complex neurodevelopmental disorders that are characterized by deficits in reciprocal social interaction and communication, as well as the presence of repetitive behaviors and highly restricted interests. Although the allelic ASD architecture remains to be fully clarified, there is definitive evidence of a high degree of locus heterogeneity and a contribution from rare and *de novo* variants.[1] However, determining a contributing role from low-frequency variants is challenging, particularly for variants that are transmitted in a non-Mendelian manner, carry intermediate risks and are present in conjunction with a tremendous amount of apparently neutral rare variations in the human genome.[2–4]

Reprogramming somatic cells to a pluripotent state by transient overexpression of specific factors enables the development of neuronal models of genomes that are predisposed to human diseases.[5] We recently demonstrated the utility of induced pluripotent stem cells (iPSCs) for investigating the functional consequences of mutations in the gene encoding the methyl CpG binding protein-2 (*MeCP2*) in neurons from patients with Rett syndrome (RTT), a syndromic form of ASD.[6,7] Neurons derived from RTT–iPSCs display several alterations compared with the controls, such as increased frequency of *de novo* L1 retrotransposition, decreased soma size, altered dendritic spine density and reduced excitatory synapses. Therefore, functional studies using neuronal cultures derived from iPSCs from ASD individuals are an important tool to explore the contribution of rare variants to ASD etiology. Furthermore, by capturing the genetic heterogeneity of ASDs, the iPSC model may clarify whether ASD individuals carrying distinct mutations in disparate genes share common cellular and molecular neuronal phenotypes.

Here, we characterize the breakpoints of a *de novo* balanced translocation t(3;11)(p21;q22) in an ASD individual that disrupts the *TRPC6* gene. *TRPC6*, a gene not previously implicated in ASD, encodes for the canonical transient receptor potential 6 channel, a voltage-independent, Ca^{2+}-permeable cation channel involved in dendritic spine and excitatory synapse formation.[8,9] The biological impact of the genetic alteration in the index case and its

[1]Department of Pediatrics/Rady Children's Hospital San Diego, Department of Cellular and Molecular Medicine, Stem Cell Program, University of California San Diego, School of Medicine, La Jolla, CA, USA; [2]Departamento de Genética e Biologia Evolutiva, Centro de Estudos do Genoma Humano, Instituto de Biociências, Universidade de São Paulo, São Paulo, SP, Brasil; [3]Department of Pediatrics, Yale University School of Medicine, New Haven, CT, USA; [4]Division of Biological Sciences, Kavli Institute for Brain and Mind, University of California San Diego, La Jolla, CA, USA; [5]Program on Neurogenetics, Child Study Center, Departments of Genetics and Psychiatry, Yale University School of Medicine, New Haven, CT, USA; [6]Departments of Genetics and Internal Medicine, Howard Hughes Medical Institute, Yale University School of Medicine, New Haven, CT, USA; [7]Instituto de Psiquiatria do Hospital das Clínicas, Faculdade de Medicina, Universidade de São Paulo, São Paulo, Brasil; [8]Walther-Straub-Institute for Pharmacology and Toxicology, Ludwig-Maximilians-Universität München, Munich, Germany; [9]Institute for Cell Engineering, The Solomon H Snyder Department of Neuroscience/Neurology, Johns Hopkins University School of Medicine, Baltimore, MD, USA; [10]Department of Pediatrics/Rady Children's Hospital San Diego, Department of Neurosciences, University of California San Diego, School of Medicine, La Jolla, CA, USA and [11]Laboratory of Genetics, The Salk Institute for Biological Studies, La Jolla, CA, USA. Correspondence: Dr AR Muotri, Department of Pediatrics/Rady Children's Hospital San Diego, Department of Cellular and Molecular Medicine, Stem Cell Program, University of California San Diego, School of Medicine, 2880 Torrey Pines Scenic Road, Sanford Consortium, Room 3005, La Jolla, CA 92093-0695, USA.
E-mail: muotri@ucsd.edu
[12]These authors contributed equally to this work.
Received 24 March 2014; revised 15 September 2014; accepted 17 September 2014; published online 11 November 2014

functional relationship to ASD etiology was evaluated through several analyses using the affected individual's dental pulp cells (DPCs), mouse models and neural cells derived from iPSCs. To test the hypothesis that different ASD-related variants can produce similar biological effects, we compared the neuronal phenotypes of iPSC-derived neurons from the TRPC6-mutant (TRPC6-mut) individual with those of patients with RTT syndrome. Finally, we conducted a large-scale case–control sequence analysis of *TRPC6*, which revealed a significant association of mutations in this gene with ASD.

MATERIALS AND METHODS

For more detailed information, please refer to Supplementary Methods.

Patient ascertainment

ASD individual F2749-1 (TRPC6-mut). The 8-year-old proband is the only child of non-consanguineous healthy parents. He was born at term after an uncomplicated pregnancy with no malformations recognized at birth. He was noted to have delayed motor skills development and poor social responsiveness and was brought for medical examination at 2 years of age. His hearing was tested and was found to be normal. He did not suffer from any other chronic medical conditions, and there was no history of head trauma or seizure. On examination, the individual met the DSM-IV criteria for autistic disorder, and the diagnosis was supported by the administration of the Childhood Autism Rating Scale. The electroencephalogram and magnetic resonance imaging were normal. The individual did not have dysmorphic features, except for synophrys, which is also present in other members of the father's family. A molecular test for Fragile-X syndrome was normal. Karyotype analysis revealed a balanced translocation (46, XY, t [3;11] [p21;q22]) in the proband that was not found in the parents. Parenthood was confirmed through genotyping of microsatellite markers.

Controls. As controls, we used six non-affected individuals that are non-related to the individual. Cells from two control individuals (USC1 and P603) were selected for reprogramming follow-up studies. This project was approved by the ethics committees of the institutes at which the study was conducted. After a complete description of the study, written informed consent was provided by the parents.

Analysis of genomic copy number variations

Genomic DNA was hybridized to the HumanHap300 Genotyping BeadChip from Illumina (La Jolla, CA, USA) according to the manufacturer's protocol to detect possible copy number variants (CNVs) in the ASD individual. The data were analyzed using PennCNV[10] and QuantiSNP[11] software, and the results were compared with the database of genomic variants (http://projects.tcag.ca/variation/) to classify the identified CNVs as rare or common variants.

Fluorescent *in situ* hybridization

Chromosomes for fluorescent *in situ* hybridization analysis were prepared from colchicine-treated lymphocytes of the proband. Bacterial artificial chromosomes encompassing the genomic regions of interest were selected from the RPCI-11 library (Roswell Park Cancer Institute, Buffalo, NY, USA) using the UCSC genome browser (http://genome.ucsc.edu/, assembly March 2006, NCBI36/hg18). The bacterial artificial chromosomes were fluorescently labeled by nick translation and hybridized to the metaphase spreads using standard protocols.[12]

Exome sequencing

Exome sequencing and analysis were performed by BGI Tech (Shenzhen, China). Briefly, genomic DNA samples were randomly fragmented into segments with a base-pair peak of 150–200 bp, and library enrichment for exonic sequences was performed using Agilent SureSelect Human All Exon 51 M (for individual and mother) or Agilent SureSelect Human All Exon 71 M (Agilent Technologies, Santa Clara, CA, USA; for the father). The captured libraries were loaded on Hiseq2000, and the sequences of each individual were generated as 90-bp paired-end reads. The coverage for the three individuals was 80-fold. Burrows-Wheeler Aligner was used for the alignment. Single-nucleotide polymorphisms (SNPs) were identified by SOAPsnp, small insertion/deletion (InDels) were detected by Samtools/GATK, and single -nucleotide variants were detected by 1/35 Varscan.

Isolation and culture of human DPCs

DPC lineages were obtained as described elsewhere.[13] Briefly, dental pulp tissues were digested in a solution of 0.25% trypsin for 30 min at 37 °C. The cells were cultivated in Dulbecco's modified Eagle's medium/F12 media (Gibco, Life Technologies, Carlsbad, CA, USA) supplemented with 15% fetal bovine serum (Hyclone, Logan, UT, USA), 1% penicillin/streptomycin and 1% non-essential amino acids and maintained under standard conditions (37 °C, 5% CO_2). The DPC control lineages used for the whole-genome expression analysis were donated by Dr Daniela Franco Bueno and Gerson Shigueru Kobayashi of the University of São Paulo. One of the DPC control lineages used for iPSC generation was a kind gift from Dr Songtao Shi (University of Southern California).

RNA extraction

RNA samples were extracted from lymphocytes, DPCs and iPSCs using Trizol reagent (Life Technologies) and treated with Turbo DNA-free (Ambion, Austin, TX, USA). Sample concentrations and quality were evaluated using a Nanodrop 1000 (Thermo Fisher Scientific, Waltham, MA, USA) and gel electrophoresis.

Microarray studies

For microarray experiments, 100 ng of RNA was converted to complementary DNA (cDNA), amplified, labeled and hybridized to the Human Gene 1.0ST chip from Affymetrix (Santa Clara, CA, USA), following the manufacturer's protocol. The chips were scanned using the GeneChip Scanner 3000 7G System (Affymetrix) and a quality control was processed using Affymetrix Expression Console Software. The data were normalized using the robust multi-array average method,[14] and the differentially expressed genes were selected with the significance analysis of microarrays method[15] and RankProd.[16] To select differentially expressed genes (DEGs), we used a P-value < 0.05 adjusted for the false discovery rate and 3000 permutations. Functional annotation, canonical pathways and networks analyses were performed using Ingenuity Pathways (http://www.ingenuity.com/). The CREB-target genes database (http://natural.salk.edu/CREB/search.htm)[17] was used to determine whether the DEGs found are regulated by the transcription factor CREB. All microarray data were deposited at GEO (GSE62632).

Gene expression analyses by quantitative PCR (qPCR)

RNA samples were reversed transcribed into cDNA using the Super Script III First Strand Synthesis System (Invitrogen) according to the manufacturer's instructions. The reactions were run on an Applied Biosystem 7500 sequence detection system using SYBR Green master mix (Applied Biosystems, Foster City, CA, USA). The primers were designed using PrimerExpress v. 2.0 software (Applied Biosystems), and specificity was verified by melting curve analysis using 7500 System SDS v. 1.2 Software (Applied Biosystems). Quantitative analysis was performed using the comparative threshold cycle method.[18] GeNorm (medgen.ugent.be/genorm/) was used to determine the stability of the reference genes *GAPDH*, *HPRT1*, *SDHA* and *HMBS* and to generate a normalization factor for the expression values of the target genes. The principles of analysis of geNorm have been described.[19] Microarray validation was performed using the one-tailed unpaired t-test with Welch's correction to compare the qPCR expression values obtained for the ASD individual and controls. A concentration of 10 μM hyperforin was used to treat the DPCs of a control sample for 15 and 30 min and 1, 3, 6, 24 and 48 h. The samples were prepared in triplicate, and the results were normalized by the values obtained for an untreated sample. Primers used on this work are described in Supplementary Table S1.

Western blotting

Rabbit anti-TRPC6 (ProScience, ProSci-Inc, Poway, CA, USA, 1:250; Sigma, St Louis, MO, USA, 1:1000); mouse anti-TRPC6 (Abcam, Cambridge, MA, USA, 1:1000); rabbit anti-CREB (Cell Signaling, Danvers, MA, USA, 1:500); rabbit anti-phosphorylated CREB (anti-P-CREB; Cell Signaling, 1:500) and mouse anti-β-actin (Ambion, 1:5000) antibodies were used as primary antibodies. Horseradish peroxidase-conjugated goat anti-rabbit and goat anti-mouse (Promega, Madison, WI, USA, 1:2000) antibodies were used as secondary

antibodies. ECL Plus (Amersham, Piscataway, NJ, USA) was used for signal detection. For semiquantitative analysis of p-CREB signal, intensity was corrected with respect to CREB/β-actin relative quantification. A paired *t*-test analysis with a *P*-value < 0.05 was used to compare the control and ASD individual p-CREB signal intensity normalized data.

Cellular reprogramming

The iPSCs were obtained from the DPCs of the ASD individual and a control. Briefly, DPCs were transduced with retroviruses containing *OCT4*, *SOX2*, *KFL4* and *MYC* to induce overexpression of these genes.[5] Two days after transduction, the cells were transferred to a co-culture system with murine embryonic fibroblasts maintained with Dulbecco's modified Eagle's medium/F12 (Life Technologies), 20% Knockout Serum Replacement (Life Technologies), 1% non-essential amino acids, and 100 μM beta-mercaptoethanol and treated with 1 mM valproic acid (Sigma) for 5 days. The iPSC colonies were identified after approximately 2 weeks in this culture system, transferred to Matrigel-coated (BD Biosciences, San Jose, CA, USA) plates, and maintained in mTeSR media (Stem Cell Technologies, Vancouver, BC, Canada).

Immunocytochemistry

The cells were fixed with phosphate-buffered saline containing 4% paraformaldehyde for 10 min and then incubated at room temperature for 1 h in a blocking solution containing 5% donkey serum and 0.1% Triton X-100. The primary antibodies were incubated overnight at 4 °C, followed by incubation with secondary antibodies (Jackson ImmunoResearch, West Grove, PA, USA) for 1 h at room temperature. Images were captured with a Zeiss microscope (Carl Zeiss, Jena, Germany). The primary antibodies used included the following: Tra-1-81 (1:100, Chemicon, Temecula, CA, USA); Nanog and Lin28 (1:500, R&D Systems, Minneapolis, MN, USA); Sox2 (1:250, Chemicon); human Nestin (1:100, Chemicon); Tuj1 (1:500, Covance, Princeton, NJ, USA); microtubule-associated protein 2 (MAP2; 1:100, Sigma); vesicular glutamate transporter-1 (VGLUT1; 1:200, Synaptic Systems, Göttingen, Germany); γ-aminobutyric acid (GABA; 1:100, Sigma); Musashi (1:200, Abcam); Ctip2 (1:200, Abcam) and Tbr1 (1:200, Abcam).

Teratoma formation

iPSC colonies from five semi-confluent 100 mm dishes ($1–3 \times 10^6$ cells) were harvested after treatment with 0.5 ng ml^{-1} dispase, pelleted and suspended in 300 μl Matrigel. The cells were injected subcutaneously into nude mice; 5–6 weeks after injection, teratomas were dissected, fixed overnight in 10% buffered formalin phosphate and embedded in paraffin. The sections were stained with hematoxylin and eosin for further analysis. The protocols were approved by the University of California San Diego Institutional Animal Care and Use Committee.

Fingerprinting and karyotype

Standard G-banding karyotype and DNA fingerprinting analysis were performed by Cell Line Genetics (Madison, WI, USA).

Neuronal differentiation

The iPSC colonies were plated on Matrigel-coated (BD Biosciences) plates and maintained for 5 days in mTSeR media (Stem Cell Technologies). On the fifth day, the media was changed to N2 media (Dulbecco's modified Eagle's medium/F12 media supplemented with 1X N2 supplement (Life Technologies) and 1 μM dorsomorphin (Tocris, Ellisville, MO, USA)). After 2 days, the colonies were removed from the plate and cultured in suspension as embryoid bodies for 2–3 weeks using N2 media with dorsomorphin during the entire procedure. The embryoid bodies were then gently dissociated with accutase (Gibco), plated on Matrigel-coated dishes and maintained in DMEM/F12 supplemented with N2, B27, and FGF media (Dulbecco's modified Eagle's medium/F12 media supplemented with 0.5X N2, 0.5X B7 supplements, 20 ng ml^{-1} fibroblast growth factor and 1% penicillin/streptomycin). The rosettes that emerged after 3 or 4 days were manually selected, gently dissociated with accutase and plated in dishes coated with 10 μg ml^{-1} poly-ornithine and 5 μg ml^{-1} laminin. This neural progenitor cell (NPC) population was expanded using DMEM/F12 supplemented with N2, B27, and FGF media. To differentiate the NPCs into neurons, the cells were re-plated with 10 μM ROCK inhibitor (Y-27632, Calbiochem, La Jolla, CA, USA) in the absence of fibroblast growth factor, with regular media changes every 3 or 4 days.

Ca^{2+} influx studies

Intracellular Ca^{2+} levels were monitored using Fluo-4 AM. The cells were incubated for 45 min at 37 °C with 2.5 μM Fluo-4 AM and superfused for 5 min with Hank's balanced salt solution buffer before the beginning of the recording. A concentration of 10 μM hyperforin (a kind gift from Dr Willmar Schwabe GmbH & Co., Karlsruhe, Germany) was used in combination with 100 μM flufenamic acid (FFA; Sigma-Aldrich, St Louis, MO, USA) for TRPC6 activation. Images were captured at 6-s intervals for 30 min using a Biorad MRC 1024 confocal system (BioRad, Hercules, CA, USA) attached to an Olympus BX70 microscope (Olympus, Tokyo, Japan). The drugs were applied at the third minute using a perfusion system. A triplicate of each individual was analyzed. The average fluorescence of the individual cells was quantified and normalized to the resting fluorescence level for each cell. The plugins MultiMeasure and MeasureStacks from ImageJ (NIH, Bethesda, MD, USA) software were used to measure fluorescence intensity. The analyses were performed blinded to avoid bias.

Cell cycle analysis

A total of 1×10^6 NPCs were harvested from a single-cell suspension with phosphate-buffered saline washing buffer (phosphate-buffered saline and 1% serum) and fixed in 75% EtOH for at least 2 h at 4 °C. After washing twice with washing buffer, the cells were stained with 200 μl propidium iodine solution (20 μg ml^{-1} propidium iodide, 200 μg ml^{-1} RNase A and 0.1% Triton X-100). Multiple NPC samples from the TRPC6-mut individual and controls were analyzed by fluorescence-activated cell sorting on a (BD Biosciences, San Jose, CA, USA), and cell cycle gating was examined using FLOWJO-Flow Cytometry Analysis Software (Tristar, Ashland, OR, USA).

Quantification of neuronal morphology and synaptic puncta

Neuronal tracing was performed on neurons for which the shortest dendrite was at least three times longer than the cell soma diameter using a semi-automatic ImageJ plugin (NeuronJ, NIH, Bethesda, MD, USA). Spines and VGLUT1 puncta were quantified after three-dimensional reconstruction of z-stack confocal images. The same density of neurons was plated in each condition. Final cell density was confirmed by 4,6-diamidino-2-phenylindole and synapsin-enhanced green fluorescent protein (EGFP)-positive cells. Only synapsin-EGFP-positive neurons with spines were scored. Images were taken randomly for each individual and from two different experiments, using at least two different clones. Quantification was performed blind to the cell genotype. The total dendritic length includes the summed length of all dendrites per neuron and dendritic segment count represents the total number of dendritic segments per neuron. No distinction was made between different types of spines because of the unviability of this assessment using the presented method. All experiments were performed with independent clones and different controls. All analyses were performed blinded to avoid bias. For the rescue experiments, 10 ng ml^{-1} insulin-like growth factor-1 (IGF-1; Peprotech, Rocky Hill, NJ, USA) or 0.5 μM hyperforin was added to neuronal cultures for 2 weeks.

Chromatin immunoprecipitation (ChIP) assay

ChIP assays were performed following the manufacturer's protocol using a ChIP assay kit (Active Motif, Carlsbad, CA, USA). The antibodies used were anti-MeCP2 and IgG (both from Upstate, Millipore, Billerica, MA, USA). We validated our antibody conditions for the ChIP assay with a previously characterized MeCP2 target, brain-derived neurotrophic factor (*Bdnf*) promoter in exon IV and a negative region in another region of the promoter region as previously described.[20,21] The input was 5% for all samples. All ChIP assays were controlled by performing parallel experiments with either no antibody or with anti-IgG pull downs. After IP, the recovered chromatin fragments were subjected to qPCR using primers for the human TRPC6 promoter region. The primers used for human TRPC6 promoter ChIP were as follows: forward primer 1, 5′-AACAGCTT GGAAACGTGGGA-3′; reverse primer 1, 5′-AAAGAGGCCAACAACCTGCT-3′; forward primer 2, 5′-TCGCAGTGACGGAAGGAAAA-3′; and reverse primer 2, 5′-AAACGCCAGATGTTCCCAGT-3′. The qPCR values were normalized to the IgG precipitation and are shown as fold enrichment. All experiments were performed in triplicate.

Construction and characterization of retroviruses

Self-inactivating murine oncoretroviruses were engineered to express short-hairpin RNAs (shRNAs) under the control of the U6 promoter and

green fluorescent protein (GFP) or the *Discosoma sp*. red fluorescent protein DsRed under the control of the Ef1 alpha promoter. shRNAs against *TRPC6* and a non-silencing scrambled control shRNA were cloned into retroviral vectors as previously described.[22] The following shRNA sequences were selected and cloned into retroviral vectors:

shRNA-control, 5′-TTCTCCGAACGTGTCACGT-3′; shRNA-TRPC6-1, 5′-TCGAG GACCAGCATACATG-3′; and shRNA-TRPC6-3, 5′-CTCAGAAGATTATCATTTA-3′.

For rescue experiments, a resistant form of murine TRPC6 (TRPC6-WT^R) was engineered to harbor six silent mutations in the region targeted by shRNA-TRPC6-1. The TRPC6 targeting sequence was mutated from AAT CGA GGA CCA GCA TAC ATG to AAC CGC GGC CCT GCT TAT ATG by site-directed mutagenesis. The resistant form of TRPC6 was cloned into a retroviral vector driven by the ubiquitin promoter followed by a bicistronic expression of GFP and a woodchuck hepatitis virus posttranscriptional regulatory element stabilization sequence. The specificity and efficiency of shRNA-control, shRNA-TRPC6-1, shRNA-TRPC6-3 and the TrpC6-WT constructs were verified by co-transfection into HEK-293 cells. Cell lysates were collected and analyzed by western blot analysis with anti-TRPC6 antibodies (Sigma).

Primary hippocampal cultures

Hippocampal neuronal cultures were prepared from C57BL/6 E18 embryonic mice. Briefly, hippocampi were dissected, dissociated with trypsin and plated at a density of 300 cells mm^{-2} on glass coverslips coated with poly-L-lysine and laminin. The hippocampal neurons were maintained in Neurobasal medium (Gibco) supplemented with B27 (Life Technologies). Neurons were treated with either shRNA scramble control or shRNA targeting TRPC6 at DIV12-14 and were fixed for further analysis at DIV21.

In vivo stereotaxic injection of engineered retroviruses into the dentate gyrus of adult mouse hippocampus

High titers of engineered retroviruses were produced by co-transfection of retroviral vectors and vesicular stomatitis viral envelope into the 293 GP cell line as described previously.[23] Supernatants were collected 24-h posttransfection, filtered through 45-μm filters and ultracentrifuged. The viral pellet was dissolved in 14 μl of phosphate-buffered saline and stereotaxically injected into the hilus of anesthetized mice at four sites (0.5 μl per site at 0.25 μl min^{-1}). The following coordinates were used: posterior = 2 mm from the bregma, lateral = ± 1.6 mm, ventral = ± 2.5 mm; posterior = 3 mm from the bregma, lateral = ± 2.6 mm, ventral = ± 3.2 mm. Adult C57BL/6 mice (6–8 weeks old, female) were used for the study. All procedures followed institutional guidelines.

Immunostaining and confocal analysis

Coronal brain sections (40 μm thick) were prepared from retrovirus-injected mice. Images of GFP$^+$ cells were acquired on a META multiphoton confocal system (Carl Zeiss, Jena, Germany). Neuronal positioning was analyzed by acquiring a single-section confocal image of a GFP$^+$ cell body stained with 4,6-diamidino-2-phenylindole and assigning it to one of the four domains as illustrated. A minimum of 10 GFP$^+$ cells were randomly chosen from the each animal, and at least three animals were used for each experimental condition, as previously described.[24] Statistical significance was determined by analysis of variance. Dendritic development was analyzed by via a three-dimensional reconstruction of the entire dendritic tree from Z-series stacks of confocal images. The images were converted to two-dimensional projections for analysis of dendritic length and branch number using NIH ImageJ software and the NeuronJ plugin (NeuronJ, NIH, Bethesda, MD, USA), as described previously [24]. As a measure of arborization, Sholl analysis was performed by counting the number of dendritic crossings at a series of concentric circles at 10-μm intervals from the cell body using the Sholl analysis plugin.

Slice electrophysiology

Mice housed under standard conditions were anesthetized at 3 weeks postretroviral injection, and acute coronal slices were prepared as previously described.[25] The brains were removed and placed in an ice-cold cutting solution containing the following: 110 mM choline chloride; 2.5 mM KCl; 1.3 mM KH_2PO_4; 25 mM $NaHCO_3$; 0.5 mM $CaCl_2$; 7 mM $MgCl_2$; 10 mM dextrose; 1.3 mM sodium ascorbate; 0.6 mM sodium pyruvate and 5 mM kynurenic acid. Slices were cut into 300-μm-thick sections with a vibratome (Leica Microsystems, Wetzlar, Germany) and transferred to a chamber containing artificial cerebrospinal fluid: 125 mM NaCl; 2.5 mM KCl; 1.3 mM KH_2PO_4; 25 mM $NaHCO_3$; 2 mM $CaCl_2$; 1.3 mM $MgCl_2$; 1.3 mM sodium ascorbate; 0.6 mM sodium pyruvate and 10 mM dextrose (pH 7.4, 320 mOsm), saturated with 95% O_2, 5% CO_2 at 35 °C for 20 min. The slices were then maintained at room temperature for at least 45 min before placement in the recording chamber. The slices were maintained at room temperature and used for the following 4 h. Electrophysiological recordings were performed at 34 °C. microelectrodes (4–6 MΩ) were filled with a solution containing the following: 120 mM potassium gluconate; 15 mM KCl; 4 mM $MgCl_2$; 0.1 mM EGTA; 10.0 mM HEPES; 4 mM MgATP; 0.3 mM Na_3GTP and 7 mM phosphocreatine (pH 7.4, 300 mOsm). The whole-cell patch-clamp configuration was used in the current-clamp mode. Approximately 10–20 giga-ohm seals were obtained with borosilicate glass microelectrodes. The electrophysiological recordings were obtained at 32–34 °C. Neurons and dendrites were visualized through differential interference contrast microscopy. The data were collected using an Axon instruments 200B amplifier (Molecular Devices, Sunnyvale, CA, USA) and acquired via a Digidata 1322A (Molecular Devices) at 10 kHz.

Electrophysiology recordings using cultured human iPSC-derived neurons

Whole-cell patch-clamp recordings were performed using cells cultured in the absence of astrocytes after approximately 6 weeks of differentiation. Before the recordings, the growth media were removed and replaced with a bath solution comprising the following: 130 mM NaCl; 3 mM KCl; 1 mM $CaCl_2$; 1 mM $MgCl_2$; 10 mM HEPES and 10 mM glucose (pH 7.4) at room temperature (22–24 °C). The electrodes for whole-cell recordings were pulled on a Flaming/Brown micropipette puller (Model P-87, Sutter Instrument, Novato, CA, USA) from filamented borosilicate capillary glass (1.2 mm OD, 0.69 mm ID, World Precision Instruments, Sarasota, FL, USA). The electrodes were fire polished, and the resistance values were typically 2–5 MΩ for the voltage-clamp experiments and 7–9 MΩ for the current-clamp experiments. The pipette solution contained the following: 138 mM KCl; 0.2 mM $CaCl_2$; 1 mM $MgCl_2$; 10 mM HEPES (Na^+ salt) and 10 mM EGTA, (pH 7.4). The osmolarity of all solutions was adjusted to 290 mOsM. All chemicals were purchased from Sigma-Aldrich, with the exception of $MgCl_2$ (J.T. Baker, Phillipsburg, NJ, USA). Current traces in voltage-clamp were leak subtracted. Liquid junction potentials were nulled for each individual cell with the Axopatch 1C amplifier (Molecular Devices, Sunnyvale, CA, USA). The analyses were performed in a double-blinded manner to avoid bias.

Behavioral tests in mice

The three-chamber test was used to evaluate the social behavior of TRPC6 wild-type (WT), heterozygous (HET) and knockout (KO) mice. To evaluate repetitive behavior, the mice were initially observed for 10 min in the dark, and the time spent in grooming and freezing behavior was measured. After 5 min of habituation under a light condition, a small cage with a never-met animal was introduced to one side of the box, and an empty cage was introduced to the other side. The time spent in each chamber and the time spent during nose-to-nose interaction between the animals was measured. Adult mice (6–8 weeks old, male) with a C57BL/6 background were used for the study. At least 12 animals per group were utilized as biological replicates. The experimenter was blind to the genotypes. The data were analyzed using the non-parametric Kruskal–Wallis analysis of variance. The analyses were performed in a double-blinded manner. All procedures followed institutional guidelines.

Mutation screening of *TRPC6*

Cohorts. The clinical characteristics of the Simons simplex collection (SSC) have previously been described in detail.[26] The following exclusion criteria were used to filter the cases: (1) ineligible/ancillary status as per SSC Family Distribution List v13; (2) missing genotyping data; (3) genotyping call rate < 95%; (4) discrepancy of genotyping data with recorded gender; (5) Mendelian inconsistencies or cryptic relatedness (up to and including second-degree relatives); and (6) non-European ancestry. A total of 1041 of 1195 cases were included in the final case cohort. The National Institute of Neurological Disorders and Stroke (NINDS) Neurologically Normal Caucasian Control Panel of unrelated adult controls do not have a personal or family history (first-degree relative) of neuropsychiatric illness (http://ccr.coriell.org/Sections/Collections/NINDS/DNAPanels.aspx?PgId=195&coll=ND). Of the 953 samples from the DNA panels NDPT020, 079, 082, 084, 090, 093, 094, 095, 096, 098 and 099, 942 passed the quality control checks described above. Additional sequence data for *TRPC6* were derived from

unrelated northern European (NE) adults present in an exome-sequencing database in our laboratory. Genotyping and whole-exome data were obtained for 2076 individuals, of which 1930 passed the quality control checks described above.

Mutation screening. For 1031 SSC cases and all 942 NINDS controls, amplification of the coding exons and splice sites was performed using lymphoblastoid cell line-derived genomic DNA via multiplex PCR using RainDance Technology (Supplementary Table S2; Lexington, MA, USA). The resulting PCR products were subjected to high-throughput sequencing on a Genome Analyzer IIx (Illumina, San Diego, CA, USA) at the Yale Center for Genomic Analysis. An in-house script was used to generate a list of variants (for more details, see Supplementary Materials). Whole-exome data for 10 additional SSC cases were available and filtered for nonsynonymous singleton variants with a SAMtools SNP quality score $\geqslant 50$. Variant confirmation was performed on blood-derived genomic DNA for the cases because it was available and on lymphoblastoid cell line-derived genomic DNA for NINDS controls using conventional PCR and Sanger sequencing. Segregation analysis was performed on blood-derived genomic DNA for cases for which family members were available. Chromatograms were aligned and analyzed for variants using the Sequencher v4.9 program (Gene Codes, Ann Arbor, MI, USA). For the NE controls, whole-exome-sequencing data were filtered by the same parameters used for the 10 SSC cases: nonsynonymous singleton variants with a significance analysis of microarrays method tools SNP quality score $\geqslant 50$. No read threshold was used to maximize sensitivity over specificity. These variants were not confirmed by Sanger sequencing, but the filtering parameters typically lead to a 70% confirmation rate in our experience. Therefore, we have included the maximum possible number of variants from the NE control cohort. To obtain the exome data, genomic DNA from both the 10 SSC probands and 1930 NE controls was enriched for exonic sequences using NimbleGen capture and sequenced by the Illumina Genome Analyzer IIX or HiSeq2000. The novelty and singleton status of all variants were determined by comparing all three cohorts and screening dbSNP137 and Exome Variant Server v.0.0.15 (NHLBI GO Exome Sequencing Project (ESP), Seattle, WA, USA; URL: http://evs.gs.washington.edu/EVS/), accessed 11 January 2012. All *P*-values for mutation burden are two-tailed and calculated from Fisher's exact test.

RESULTS

Characterization of the t(3;11)(p21;q22) translocation breakpoint and exome sequencing

We identified an 8-year-old male autistic individual carrying a *de novo* 46, XY, t(3;11)(p21;q22) translocation by G-banding karyotyping of lymphoblastoid cells. No gain or loss of genetic material was observed near the breakpoint areas via a genome-wide array analysis (Figure 1a). Only a duplication (104 225 150–104 339 273-bp) on chromosome 14 was identified, which was previously shown to be a common CNV (http://projects.tcag.ca/variation/). Fluorescent *in situ* hybridization analysis revealed that bacterial artificial chromosome probes RP11-780O20 and RP11-109N8 span the breakpoint on chromosome 3p21, whereas probes RP11-3F4 and RP11-1006P7 map distal and proximal to the breakpoint, respectively (Figures 1b and c). This narrowed the breakpoint to an interval of approximately 15-kb spanning the gene encoding the Vpr-binding protein (*VPRBP*), indicating that this gene was disrupted. Similarly, the breakpoint on chromosome 11q22 was mapped to a region spanned by probes RP11-141E21 and RP11-153K15, distal to RP11-315B9 and proximal to RP11-942D19 (Figures 1d and e), suggesting disruption of the *TRPC6* gene, which was confirmed by the use of additional strategies.

We first measured the expression levels of *TRPC6* exons 4, 6, 12 and 13 in the lymphocytes of the ASD individual, his parents and six non-affected control individuals by quantitative real-time PCR (Supplementary Figure S1a). In the ASD individual's parents and in six other individual controls, exons 6, 12 and 13 had similar expression levels as exon 4. In the ASD individual, however, the expression levels of exons 12 and 13 were reduced by 60% compared with exon 4. After sequencing all *TRPC6* exons, we found that the individual was HET for two common polymorphisms: one mapping to exon 6 (rs12366144) and the other to exon 13 (rs12805398). However, sequencing of cDNA from the individual's lymphocytes revealed HET only for the polymorphism in exon 6 (Supplementary Figure S1b). Parentage was confirmed through genotyping of microsatellite markers (Supplementary Figure S1c). These results show that *TRPC6* has biallelic expression and that the HET loss in exon 13 in the individual's cDNA can be explained by *TRPC6* disruption. Accordingly, *TRPC6* is transcribed up to the breakpoint, which is located between exons 6 and 12. We did not identify any pathogenic change in *TRPC6* exons upon sequencing the individual's DNA (data not shown). We also did not identify any extra band in the protein extracts from individual's cells using a N-terminal antibody, indicating that a truncated TRPC6 form is unlikely to be a byproduct of the translocation (Supplementary Figure S1d).

Disruption of *TRPC6, VPRBP* and several other unknown genes may contribute to the ASD phenotype. To identify other genetic alterations in this ASD individual, we performed exome sequencing on the individual and compared the result with those for his parents. Exome-sequencing analysis revealed 28 *de novo,* rare, nonsynonymous variants and three frameshift insertions/deletions in the individual. Consultation with AutismKB[27] indicated that none of the other genes harboring genetic variants are associated with ASD, with the exception of the cyclic adenosine monophosphate-specific (*PDE4A*) gene, for which lower levels of expression have been observed in the brains of autistic individuals.[28] We also observed an alteration in the *ATXN3* gene, linked to the spinocerebellar ataxia-3 disease in humans. All genetic variants are presented in Supplementary Table S3.

TRPC6 disruption leads to transcriptional alterations and dysregulation of CREB phosphorylation

To determine gene transcription because of genetic perturbations in the ASD individual carrying the novel chromosomal translocation, we conducted a global expression analysis comparing the individual's DPCs to six control samples. DPCs can be easily isolated from the deciduous teeth of ASD individuals via a non-invasive procedure.[29] DPCs have an ectodermic neural crest origin, express several neuronal markers and have proven to be a useful model to study ASD.[30–32] We identified 67 DEGs between the ASD individual and non-affected controls ($P < 0.05$; Supplementary Table S4). Functional annotation analysis revealed that 16 (24%) of these genes have a role in nervous system development and function (Table 1). We confirmed the reduction of *TRPC6* expression ($P < 0.01$) but not *VPRBP* (Figure 2a). The reduced level of *TRPC6* expression is likely due to nonsense-mediated decay or rearrangement of regulatory elements caused by the translocation. Moreover, *PDE4A*, *ATXN3* and *DOCK3* (another neuronal gene[33] present near the break point on chromosome 3; Figure 1b) were also not differentially regulated in the individual's DPCs (Figure 2a). TRPC6 is a Ca^{2+}-permeable, nonselective, cation channel involved in neuronal survival, growth cone guidance, and spine and synapse formation, biological processes that have previously been implicated in ASD etiology.[8,9,34–36] The function of *VPRBP* (Vpr-binding protein) is less clear and may include DNA replication, S-phase progression and cellular proliferation.[37] Given the time-consuming nature of additional functional analyses, we elected to focus on additional genetic and functional studies of *TRPC6*, which has not been previously associated with ASDs.

Using the CREB-target genes database (http://natural.salk.edu/CREB/), we determined that 8 of the 16 functionally relevant DEGs are regulated by CREB, a transcription factor that is activated upon Ca^{2+} influx through TRPC6.[8] Of the functionally relevant DEGs, we evaluated six CREB-target genes (*INA, MAP2, NPTX1, CLDN11, PCDH10 and EPHA4*) and two other genes (*SEMA3A* and *CDH6*) by qPCR to validate the microarray experiments. We measured

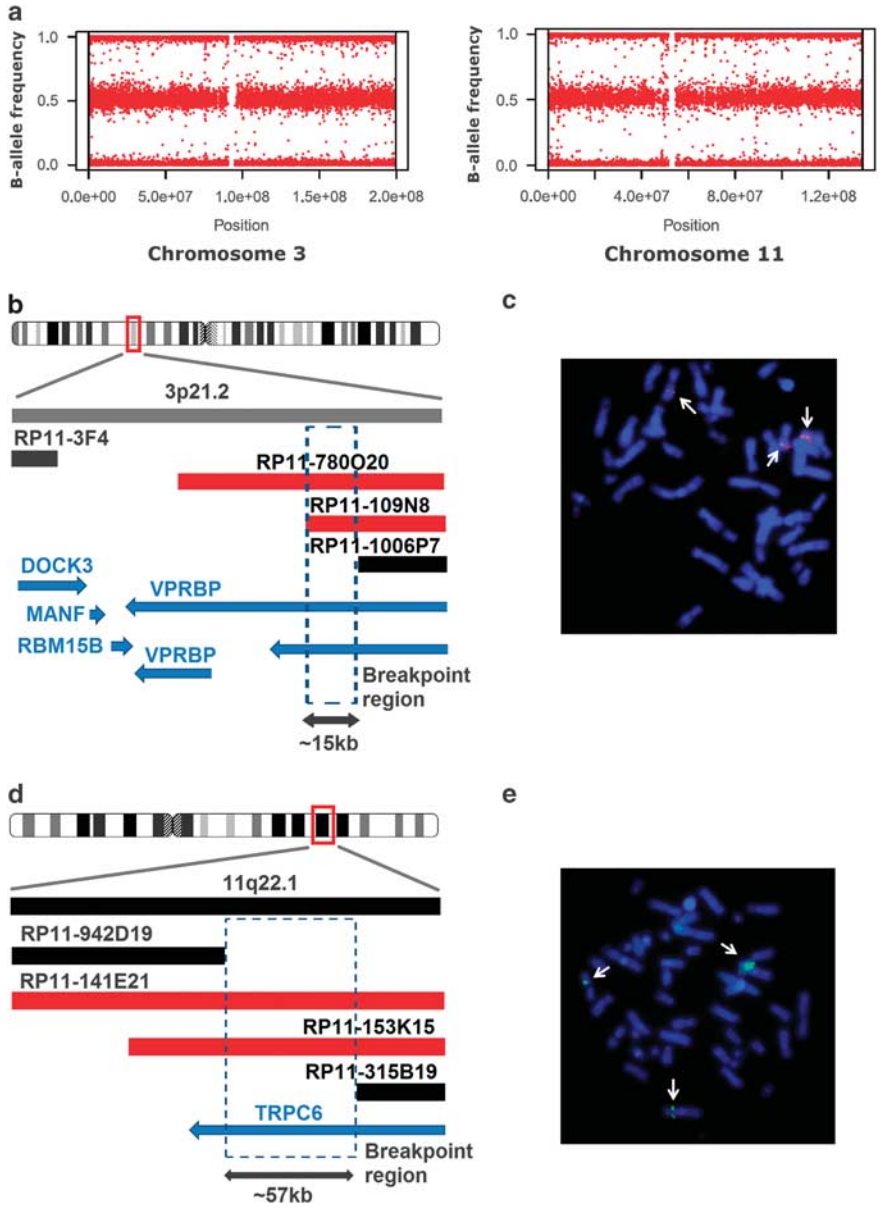

Figure 1. Mapping the breakpoints in the autism spectrum disorder (ASD) individual with the 46, XY, t(3;11)(p21;q22) karyotype. (**a**) The allele frequency distribution plot for chromosomes 3 and 11 generated by single-nucleotide polymorphism (SNP) array genotyping showed no gain or loss of genetic material on these chromosomes. (**b**) The schematic view of the bacterial artificial chromosome (BAC) probes used and the surrounding breakpoint area on chromosome 3. RP11 probes marked in red span the breakpoint, whereas the black ones do not. The shared region between probes RP11-780O20 and RP11-109N8 narrows the breakpoint area to a region inside the *VPRBP* gene. The blue arrows indicate open reading frames. (**c**) Fluorescent *in situ* hybridization (FISH) imaging showing that RP11-780O20 probe (red signal) binds to normal and derivative chromosome 3 and to derivative chromosome 11, indicating that the probe spans the breakpoint (arrows). (**d**) A schematic view of the BAC probes used and the surrounding areas on chromosome 11. A shared region between probes RP11-153K15 and RP11-141E21 places the breakpoint in *TRPC6*. (**e**) FISH image showing the BAC probe RP11-153K15 (green signal) bound to normal chromosome 11 and both derivatives chromosomes 3 and 11 (arrows).

dysregulated expression of *CDH6* (−2.68-fold, $P < 0.05$), *INA* (−2.64-fold, $P < 0.05$), *MAP2* (−2.79-fold, $P < 0.05$) and *CLDN11* (4.07-fold, $P < 0.001$) in the individual compared with the controls in the same direction observed in the microarray analysis (Table 1). To validate that *TRPC6* haploinsufficiency is leading to transcriptional dysregulation of these genes, we treated a control DPC culture with hyperforin plus FFA and measured the expression levels of the same candidate genes over 48 h (Figures 2b and c and Supplementary Figure S1e). Hyperforin specifically activates *TRPC6* and FFA increases the amplitude of the currents through this channel.[38–40] If the candidate genes are regulated through TRPC6 signaling, we expect a change in their expression levels opposite to the observed change in the TRPC6-mut individual. After a 48-h treatment, we observed the expected correlation for five of the eight genes. Although the expression levels of *SEMA3A*, *EPHA4* and *CLDN11* were significantly reduced (−28-fold, − 3.2-fold and − 4.76-fold, respectively), *MAP2* and *INA* displayed 20-fold and 10-fold increases in expression, respectively. These results validate the microarray data and support the hypothesis that the selected genes are regulated by the TRPC6 pathway.

Table 1. Selected functionally relevant genes differentially expressed between the TRPC6-mutant individual and controls

Gene	*Fold change*[a]	*Gene ontology*	*Regulation by CREB*[b]	*qPCR validation (P-value)*
INA	−2.639988194	Nervous system development; neurofilament cytoskeleton organization	ChIP-on-chip	0.0198
NPTX1	−2.855578291	Growth of neurites; synaptic transmission; central nervous system development	*In silico*	0.0885
MAP2	−2.789671289	Growth of neurites; development and elongation of neurites; patterning of cerebral cortex; polarization of hippocampal neurons	ChIP-on-chip	0.0363
EPHA4	2.362428255	Guidance of axons; formation of the pyramidal tract; axon guidance	ChIP-on-chip; *In silico*	0.4305
CLDN11	4.066602785	Axon ensheathment; calcium-independent cell–cell adhesion; migration of neuroglia	*In silico*	0.0005
PCDH10	−4.318180517	Cell adhesion; establishment and function of specific cell–cell connections in the brain	ChIP-on-chip; *In silico*	0.3331
CLDN1	4.171417178	Calcium-independent cell–cell adhesion; myelination of cells	*In silico*	
PTGS2	−3.49316255	Activation of astrocytes; activation of neuroglia; memory; positive regulation of synaptic plasticity; negative regulation of synaptic transmission, dopaminergic; positive regulation of synaptic transmission, glutamatergic	ChIP-on-chip	
CDH6	−2.675463010	Cell adhesion; establishment and function of specific cell–cell connections in the brain	No evidence	0.0418
SEMA3A	2.314408538	Nervous system development; axonal fasciculation; regulation of axon extension involved in axon guidance; distribution of neurons; migration of neuroglia; growth of neurites; chemorepulsion of sympathetic neurons	No evidence	0.1828
CASP1	2.545250054	Activation of astrocytes; activation of neuroglia	No evidence	
VCAM1	4.546975557	Growth of neurites; distribution of neurons; cell adhesion; guidance of axons	No evidence	
ACAN	−4.199956627	Growth of neurites; cell adhesion	No evidence	
CCL2	2.41655874	Cell adhesion; astrocyte cell migration	No evidence	
HGF	4.252390982	Growth of neurites; complexity of dendritic trees	No evidence	
PCDH18	2.508559732	Cell adhesion; brain development	No data available	

Abbreviations: ASD, autism spectrum disorder; ChIP, chromatin immunoprecipitation; qPCR, quantitative PCR. [a]Logarithmic gene expression difference between ASD individual and controls. [b]Evidence of gene transcription regulation by the transcription factor CREB according to the database http://natural.salk.edu/CREB/search.htm. Zhang *et al.*[17] used three different strategies to identify the genes regulated by CREB*: in silico* analysis, chromatin co-immunoprecipitation followed by microarray analysis (ChIP-on-ChIP) and expression analysis of genes induced by forskolin (array). The genes for which no evidence of CREB regulation was found are annotated as 'no evidence'; those for which no information is available in the analyzed database are annotated as 'no data available'.

We measured CREB phosphorylation in the DPCs of the individual and a control to assess the functional effect of *TRPC6* disruption. Stimulation of DPCs with hyperforin plus FFA induced a significantly reduced level of increased p-CREB in the individual's DPCs ($30.3 \pm 0.7\%$) compared with the control ($48.6 \pm 2.3\%$; $P < 0.005$) after 15 min. After 30 min, p-CREB levels in the individual's DPCs ($6.3 \pm 2.1\%$) were also significantly lower compared with the control ($20.9 \pm 2.1\%$; $P < 0.05$) (Figures 2d and e). Taken together, these results show that several of the functionally relevant DEGs identified in the microarray studies are controlled via TRPC6 signaling, likely through CREB phosphorylation, suggesting that *TRPC6* disruption influences neuronal cell function.

Generation of neural cells from ASD individuals

To further evaluate the effect of *TRPC6* haploinsufficiency on neural cell function, we generated iPSCs from DPCs from the ASD individual and two control individuals (Supplementary Figure S2 and Supplementary Tables S5 and S6). We chose to reprogram DPCs because these cells develop from the same set of early progenitors that generate neurons. Furthermore, the neurons derived from iPSCs generated from DPCs express higher levels of forebrain genes, many of which are implicated in ASD.[41] We fully characterized three clones from each individual and used at least two different clones for follow-up experiments. A summary of the clones used for each experiment can be found in Supplementary Table S6. NPCs and cortical neurons from iPSCs were obtained using a modified protocol from our previous publication.[6] Briefly, iPSC colonies on Matrigel were treated with dorsomorphin under fibroblast growth factor-free conditions until confluence. Pieces of iPSC colonies were grown in suspension for 2–3 weeks as embryoid bodies in the presence of dorsomorphin (Figure 3a). The embryoid bodies were then dissociated and plated to form rosettes. The rosettes were manually selected and expanded as NPCs (Figure 3a). These NPCs were negative for the pluripotent marker OCT4 and positive for early neural-specific markers such as Musashi-1 and Nestin (Figure 3b and Supplementary Figure S3a). To obtain mature neurons, NPCs were plated with ROCK inhibitor and maintained for 3–4 additional weeks under differentiation conditions. At this stage, the cells were positive for the pan-neuronal marker Tuj1 (β-III-Tubulin) and expressed the more mature neuronal markers synapsin I (*SYN1*) and MAP2 (Figure 3c). These cells expressed genes typically found in the cortex, including *CTIP2*, important for the differentiation of subcortical projecting neurons; *TBR1*, critical for cortical development and *ABAT*, a marker for GABAergic neurons, encoding for the 4-aminobutyrate aminotransferase protein and responsible for the catabolism of GABA neurotransmitter (Supplementary Figure S3a). Expression of *NESTIN* indicates the presence of NPCs and the expression of *S100B* and *GFAP* are indicative of glia cells, suggesting a mixed cell population at this stage (Supplementary Figure S3a). In our cultures, the presynaptic SYN1 puncta were frequently adjacent to the postsynaptic marker HOMER1, suggesting the presence of developed synapses (Supplementary Figure S3b). Using immunostainning, we also detected expression of the inhibitory neurotransmitter GAB) in 13% of the neurons, and 22%

were positive for VGLUT1, a marker for excitatory neurons, in both controls and ASD subjects (Figures 3c–e). Our protocol generated a consistent population of forebrain neurons, confirmed by the colocalization of pan-neuronal and subtype-specific cortical markers, such as 16% of Ctip2 (layers V and VI) and 6% of Tbr1 (layers I and VI; Figures 3d and e). Expression of peripherin and En1, markers for peripheral and midbrain neurons, respectively, was not detected. We did not observe a significant variability in these subtypes of neurons between the control and ASD backgrounds (Supplementary Figure S3a). Next, we determined the functional maturation of the iPSC-derived neurons using electrophysiological methods. Whole-cell recordings were performed using cells that had differentiated for at least 6 weeks in culture. Both controls and ASD neurons showed action potentials evoked by somatic current injections (Figures 3f–h and Supplementary Figures S3c and d). Therefore, our data indicate that somatic cell reprogramming did not affect the ability of iPSC-derived neurons to mature and become electrophysiologically active.

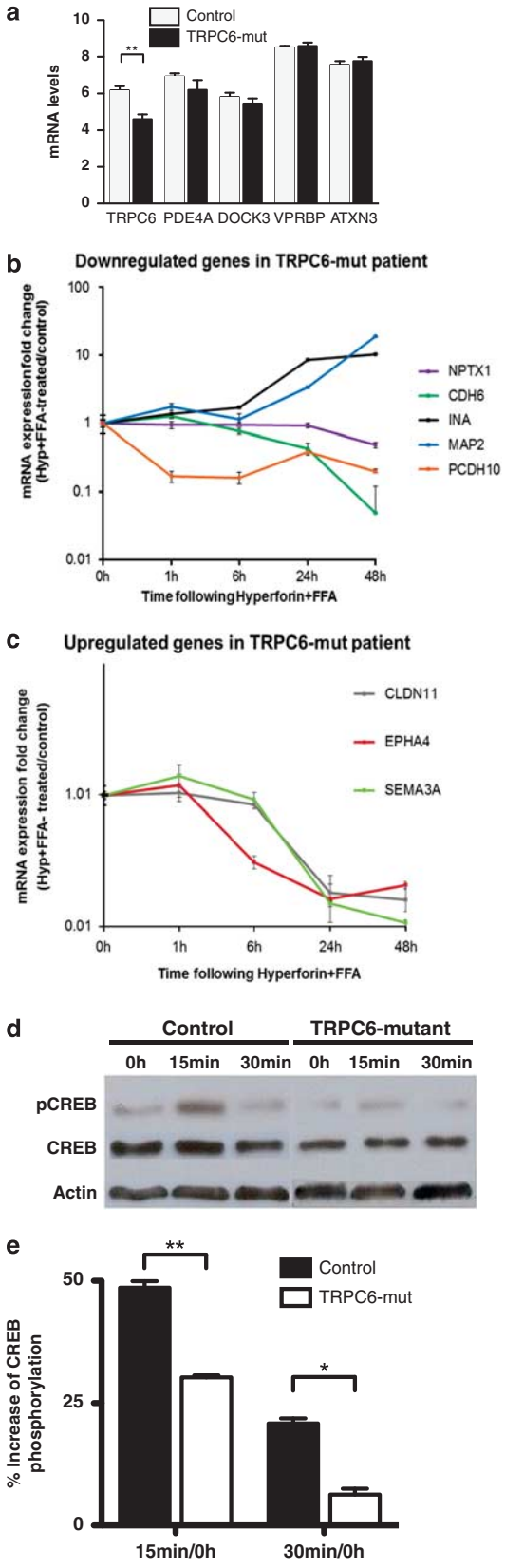

TRPC6 disruption does not affect NPC proliferation

TRPC1, another member of the transient receptor potential channel family, is involved in NPC proliferation mediated by fibroblast growth factor.[42] Therefore, we investigated whether reduction of *TRPC6* expression levels affects the cell cycle profile. No difference was observed when comparing the percentage of cells in G1 ($56.2 \pm 5.0\%$ and $47.8 \pm 10.5\%$, $P > 0.2$), S ($30.6 \pm 3.0\%$ and $36.0 \pm 6.4\%$, $P > 0.2$) and G2/M ($10.1 \pm 1.4\%$ and $14.3 \pm 4.8\%$; $P > 0.2$) phases between control and TRPC6-mut iPSC-derived NPCs, indicating that *TRPC6* likely does not have a role in NPC proliferation, in contrast to *TRPC1* (Supplementary Figure S4a).

Ca^{2+} influx is reduced in TRPC6-mut NPCs

The role of *TRPC6* in dendritic spine formation depends on a pathway that involves Ca^{2+} influx through the channel.[8] To test if changes in intracellular Ca^{2+} levels may be altered in TRPC6-mut neural cells upon TRPC6 activation, we stimulated iPSC-derived NPCs from the TRPC6-mut individual and a control with hyperforin plus FFA. This combination of drugs induced transient and repetitive increases in intracellular Ca^{2+} concentrations in both TRPC6-mut- and control-derived NPCs. The TRPC6 activation-induced Ca^{2+} oscillation peak was significantly higher in control NPCs compared with TRPC6-mut NPCs (Figure 4a). The average amplitude of the Ca^{2+} increase over baseline in the 100 cells analyzed was reduced by 30% in the TRPC6-mut NPCs (1.9 ± 0.08-fold) compared with the control sample (2.7 ± 0.2-fold; $P < 0.001$) when stimulated with hyperforin and FFA (Figure 4b).

TRPC6 signaling regulates gene expression in neuronal cells

To validate our DPC findings, we examined the expression of some neuronal genes in NPCs in response to TRPC6 activation (Supplementary Figure S4b). After a 48-h hyperforin treatment, *SEMA3A* expression was reduced (0.6 ± 0.05-fold, $P < 0.05$), whereas *INA* and *MAP2* again showed increased expression (2.6 ± 0.09-fold and 1.8 ± 0.1-fold; $P < 0.001$). These results parallel

Figure 2. TRPC6 channels regulate the expression of neuronal development genes. (**a**) Differential gene expression in the controls and autism spectrum disorder (ASD) individual cells of candidate genes located in the translocation region or detected by exome sequencing. Only *TRPC6* displayed a significant reduction in mRNA levels ($P < 0.01$). (**b**) Decreasing expression of candidate genes upon TRPC6 stimulation with hyperforin/flufenamic acid (FFA). (**c**) Genes upregulated in the TRPC6-mut genetic background after hyperforin/FFA treatment. (**d**) Representative western blot showing increased CREB phosphorylation after 15 and 30 min of hyperforin stimulation normalized to non-stimulated cells. (**e**) The level of CREB phosphorylation in dental pulp cells (DPCs) from the TRPC6-mut individual after TRPC6 activation with hyperforin is significantly lower compared with the control sample ($n = 3$, $P < 0.05$; *t*-test). The error bars in all panels show the s.e.m. $^*P < 0.05$; $^{**}P < 0.01$.

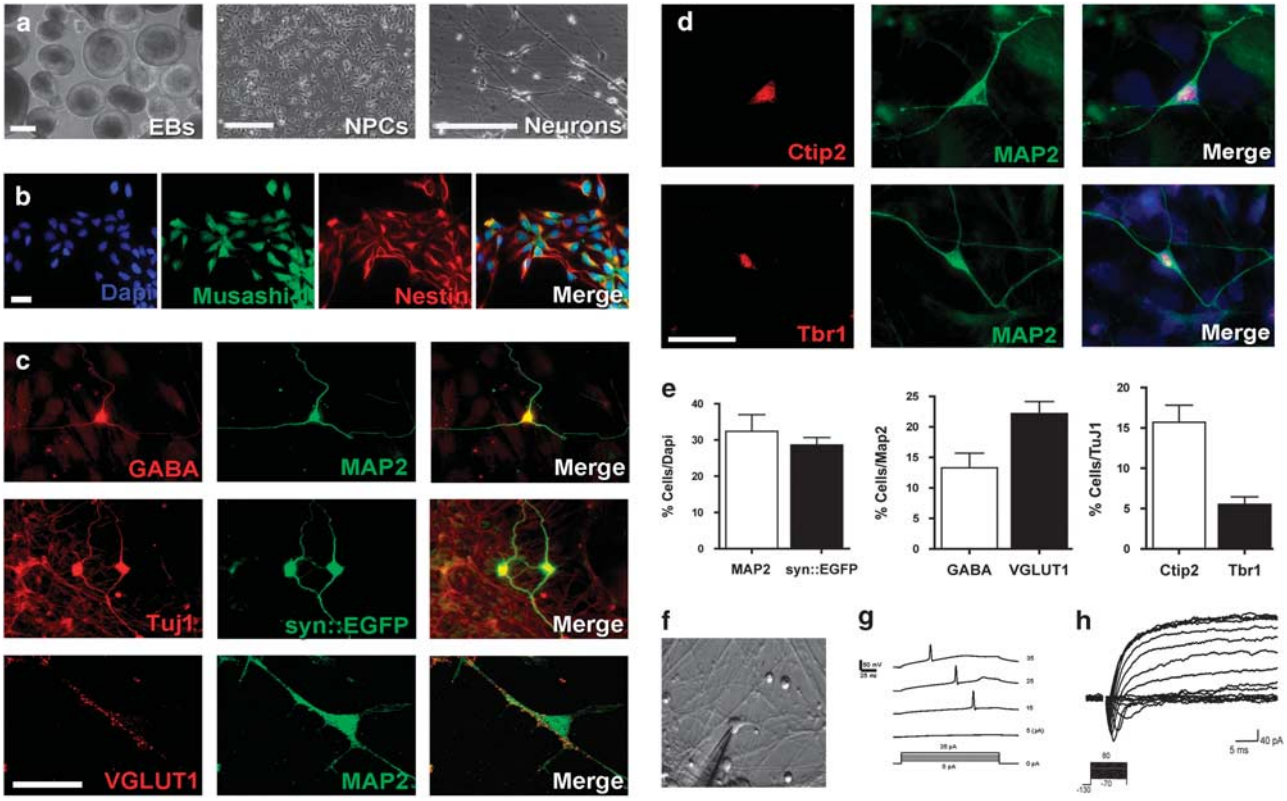

Figure 3. Derivation of neural progenitor cells (NPCs) and neurons from induced pluripotent stem cells (iPSCs). (**a**) Representative images depicting morphological changes during neuronal differentiation from control and TRPC6-mut iPSCs. Bar = 100 μm. (**b**) NPCs are positive for the neural precursor markers Musashi-1 and Nestin. Bar = 50 μm. (**c**) Representative images of cells after neuronal differentiation. iPSC-derived neurons express neuronal markers such as γ-aminobutyric acid (GABA), microtubule-associated protein 2 (MAP2) and synapsin I. (**d**) Examples of distinct cortical neuronal subtypes present differentiating cultures after 3 weeks. Bar = 30 μm. (**e**) We obtained 30% neurons in our cultures with this protocol, as measured by MAP2 staining and infection with the syn::enhanced green fluorescent protein (EGFP) lentiviral vector. Most MAP2-positive cells expressed vesicular glutamate transporter-1 (VGLUT1), in contrast with 12% of neurons expressing GABA. Ctip2-positive neurons were more abundant (16%), whereas Tbr1-positive neurons were present in a small percentage in the population (6%) at the end of the differentiation protocol. (**f**) Morphology of neurons patched for electrophysiological recording. (**g**) Representative recordings of evoked action potentials in iPSC-derived neurons in response to current steps under current patch clamps. (**h**) Representative Na^+ and K^+ currents in iPSC-derived neurons. The error bars in all panels show the s.e.m.

our DPC expression analysis and support the hypothesis that TRPC6 signaling is important for the regulation of genes involved in neuronal function.

TRPC6 disruption alters the neuronal phenotype

To determine if *TRPC6* disruption influences spine formation and synaptogenesis, we investigated neurons derived from TRPC6-mut and control iPSCs. To avoid variability from reprogramming, all experiments were performed with different iPSC clones and independent experiments. All biological replicates and iPSC clones used in each experiment are summarized in Supplementary Table S6. The neurons derived from this ASD individual exhibited a 60% reduction ($P < 0.01$) in *TRPC6* protein levels as measured by western blot (Figures 4c and d). We first examined neuron morphology by infecting cells with a previously described lentiviral vector containing the EGFP sequence under the control of the synapsin gene promoter (syn::EGFP).[6] By measuring the size of neurites and their ramifications, we verified that the TRPC6-mut neurons are shorter in total length (1782 ± 101.2 and 2666 ± 153.7 pixels; $P < 0.001$) and less arborized (3.7 ± 0.2 and 8.7 ± 0.5 vertices; $P < 0.001$) than the controls (Figures 4e–g). Moreover, the density of dendritic spines in TRPC6-mut neurons was reduced (7.4 ± 0.5 spines per 20 μm of dendrite length) compared with control neurons (12.9 ± 0.8 spines; $P < 0.001$) derived from several individuals (Figures 4h–j, Supplementary Figure S3e). *TRPC6* expression was previously shown to regulate spine density.[8] Thus, to confirm that the alterations observed in this ASD individual were caused by TRPC6 haploinsufficiency, we downregulated *TRPC6* expression in control neurons using a specific, prevalidated shRNA in a lentiviral vector. Neurons derived from control iPSCs expressing shTRPC6 exhibited a significant reduction in spine density (6.0 ± 0.5 spines) compared with control neurons expressing a scrambled shRNA (12.5 ± 0.7 spines; $P < 0.0001$; Figure 4j). Even further, restoring *TRPC6* expression in the TRPC6-mut neurons using a lentiviral vector expressing WT *TRPC6* (Supplementary Figures S4c and d) rescued these morphological alterations, increasing total neuronal length (3051 ± 133.4 pixels; $P < 0.001$), arborization (8.9 ± 0.6 vertices; $P < 0.001$) and dendritic spine density (11.9 ± 0.9 spines; $P < 0.001$) to control levels (Figures 4e, f and h). Interestingly, the specific activation of the WT *TRPC6* in mutant neurons by hyperforin was also sufficient to rescue these morphological phenotypes in our culture conditions (Figures 4e, f and h).

TRPC6 is mainly expressed in glutamatergic synapses and its loss interferes with synapsin I cluster density in presynaptic sites of hippocampal neurons, suggesting that this gene has an important role in the regulation of excitatory synapse strength.[9] Quantifying

VGLUT1 puncta in MAP2-labeled neurons confirmed that the TRPC6-mut neurons had a significantly lower density of VGLUT1 puncta (4.6 ± 0.3 puncta per 20 µm of dendrite length) compared with independent clones isolated from several independent controls (10.3 ± 0.4 puncta; $P < 0.001$) (Figures 4k and l, Supplementary Figure S3g). To determine if *TRPC6* haploinsufficiency contributed to the lower density of VGLUT1 puncta, we treated TRPC6-mut neurons with hyperforin to specifically stimulate *TRPC6*. After 2 weeks of treatment, the neurons exhibited a significant increase in the number of VGLUT1 puncta compared with untreated cells (7.4 ± 0.5 puncta; $P < 0.05$) (Figure 4k). Control neurons expressing shTRPC6 also exhibited a lower density of VGLUT1 puncta, indicating that loss of *TRPC6* function affects the formation of glutamatergic synapses ($P < 0.01$) (Figures 4m and n). In addition, overexpression of TRPC6 in the TRPC6-mut neurons was able to rescue synapse numbers (8.0 ± 0.6 puncta per 20 µm of dendrite length; $P < 0.001$) to control levels, as measured by synapsin I puncta (Figures 4o and p). Finally, electrophysiological recordings revealed that the Na^+ currents of TRPC6-mut neurons (28.38 ± 7.5 pA) were impaired compared with the controls (154.4 ± 45.9 pA; $P < 0.0001$) (Figures 4q and r, Supplementary Figure S3e).

TRPC6 and MeCP2 share a similar molecular pathway

Certain neuronal phenotypes (reduction of spine density and glutamatergic synapses) associated with TRPC6 function loss are similar to those previously described for loss of MeCP2 function in human neurons.[6] MeCP2 genetic alterations have been recognized in several non-syndromic ASD individuals,[43–50] and reduced MeCP2 expression in brains of autistic individuals has been reported.[51,52] In addition, two independent studies have reported that MeCP2 regulates *TRPC6* expression in the mouse brain, likely through an indirect mechanism.[53,54] Thus, we investigated whether MeCP2 acts upstream of *TRPC6* in human neurons. We used two iPSC clones from a female RTT patient carrying the T158M MeCP2 mutation, which results in persistent X chromosome inactivation.[6] Each clone expresses a different MeCP2 allele, a WT or mutant version of the *MeCP2* gene. We then differentiated both clones into neurons and evaluated TRPC6 protein expression levels. The TRPC6 expression level was reduced by 40% in the clone carrying the non-functional version of MeCP2 compared with the WT control clone (61.67 ± 6.0% and 99.3 ± 1.2%; $P < 0.01$), indicating that MeCP2 levels affect *TRPC6* expression in human neurons (Figure 4s). This observation supports MeCP2 acting upstream of *TRPC6* in the same molecular pathway to affect

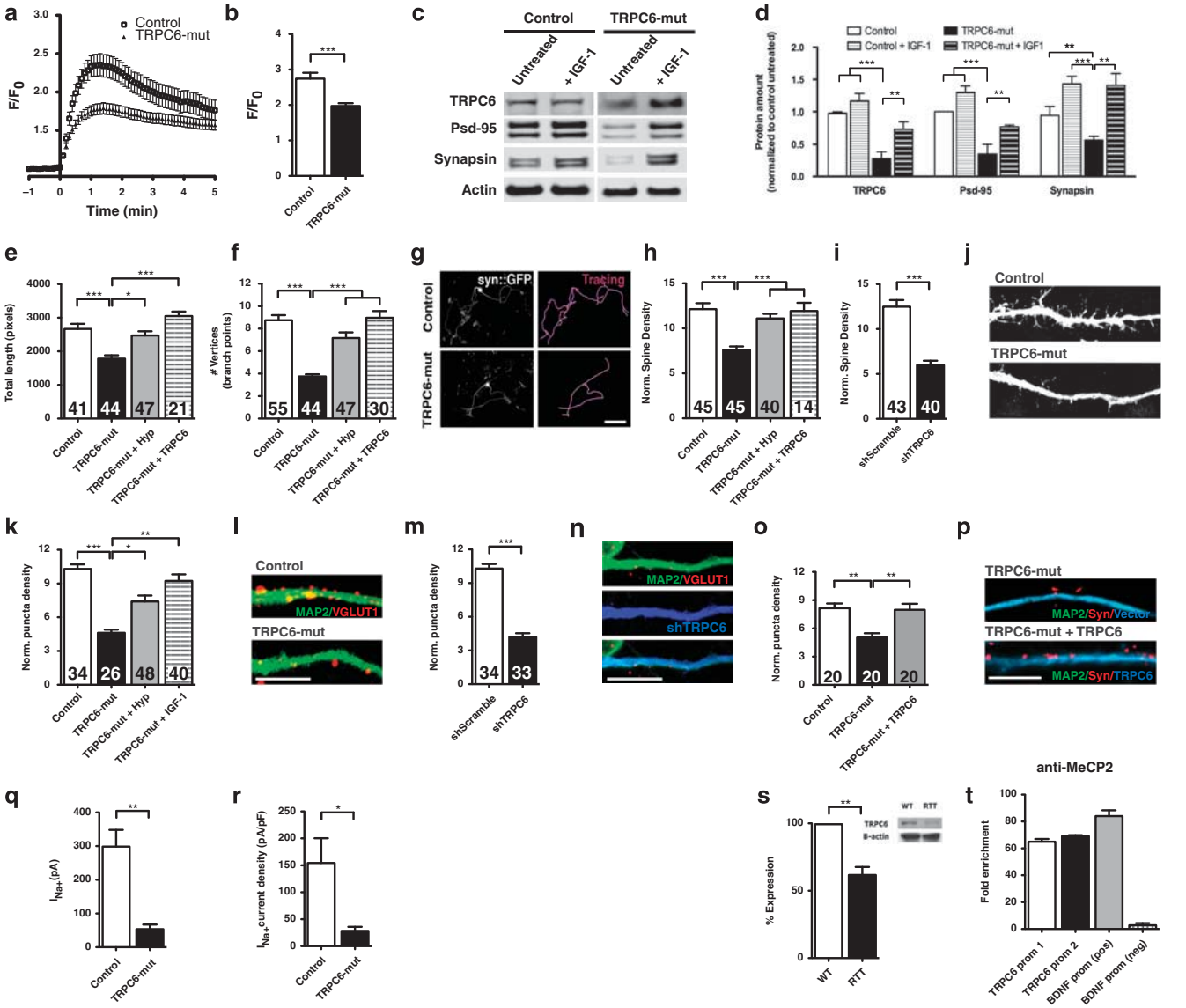

Figure 4. See for caption on page 1360.

neuronal morphology and synapse formation. We next investigated whether MeCP2 could occupy regions of the human *TRPC6* promoter. ChIP followed by qPCR revealed high levels of MeCP2 in association with the *TRPC6* promoter region in human neurons, suggesting a potential mechanism of transcriptional regulation (Figure 4t, Supplementary Figure S4f).

Our data suggest that the molecular pathway involving MeCP2 and *TRPC6* is a rate-limiting factor in regulating glutamatergic synapse number in human neurons. Administration of IGF-1 promotes the reversal of RTT-like symptoms in a mouse model[55] and of molecular alterations in RTT human neurons,[6] and is currently in clinical trials for RTT patients.[56] To investigate whether the potential convergence of molecular mechanisms underlying RTT and non-syndromic autism suggests shared therapeutic benefits, we treated TRPC6-mut neurons with full-length IGF-1 (10 ng ml^{-1}). Interestingly, we observed a significant increase in TRPC6 protein levels after treatment. Moreover, Psd-95 and synapsin I protein levels were also upregulated by IGF-1 ($P < 0.01$; Figures 4c and d). IGF-1 treatment also rescued the glutamatergic synapse number in TRPC6-mut neurons as measured by VGLUT1 puncta (9.2 ± 0.6 puncta per 20 μm of dendrite length; $P < 0.01$), suggesting that the drug treatment could correct this neuronal phenotype (Figure 4k).

TRPC6 downregulation compromises neuronal development *in vivo*

In vitro experiments in rodent primary neurons have shown that Trpc6 levels affect spine density and excitatory synapses.[9,57] To corroborate our findings from human-derived neurons, we looked to examine the effect of *Trpc6* loss in a rodent model. We validated two shRNAs (#1 and #3) against mouse *Trpc6* by western blot analysis and used both for further experiments (Supplementary Figures S4g and h). Using this shRNA targeting *Trpc6*, we transduced mouse primary hippocampal neurons. The neurons expressing shRNA targeting *Trpc6* demonstrated reduced spine density (7.5 ± 0.5 and 11.4 ± 0.8 spines per 20 μm of dendrite length; $P < 0.001$) and fewer synapses (5.6 ± 0.5 and 7.7 ± 0.5 puncta per 20 μm of dendrite length; $P < 0.01$) versus neurons transduced with a shRNA scramble control (Figures 5a and b). Thus, as described above, we determined that TRPC6 downregulation causes similar neuronal alterations in human and rodent neurons. We next looked to validate the cell autonomous effect of *TRPC6* loss-of-function *in vivo* by taking advantage of adult neurogenesis in the hippocampus.[58] Using retroviruses to target newborn neurons, we delivered the shRNAs against mouse *Trpc6*. *Trpc6* downregulation led to migration defects and reduced neuronal dendritic arborization (Figures 5c–f). Moreover, whole-cell patch clamping to record action potentials revealed a significant reduction in the firing rate of neurons expressing shRNAs against *Trpc6* compared with the controls (Figures 5g–i). To demonstrate the contribution of *Trpc6* to these phenotypes *in vivo*, we rescued the migration defects by co-transfecting the shRNA with an expression construct for an shRNA-resistant form of TRPC6-WT (TRPC6-WT^{R}; Figure 5d, Supplementary Figure S4h).

TRPC6 KO mice [59] display reduced exploratory activity in a square open field and elevated star maze compared with control siblings.[60] Limited environmental exploration is commonly associated with ASD individuals.[61] Thus, we decided to investigate whether the TRPC6 KO mouse displays other ASD-like behaviors. We assessed the social interaction and repetitive behaviors of these animals, but observed no significant differences between WT controls and HETs or WT and KO mice (Figure 5j). Together, these data demonstrate loss or reduction of TRPC6 in a rodent model induces neuronal abnormalities paralleling our findings in the TRPC6-mut iPSC-derived neurons, such as reduced neuronal arborization, spine density and synapse numbers.

Mutation screening of TRPC6

Based on the initial observation of *TRPC6* disruption by a chromosomal breakpoint, we established a narrow hypothesis

Figure 4. Alterations in neural cells derived from the TRPC6-mut individual. (**a**) Ca^{2+} influx dynamics through TRPC6 channels activated by hyperforin plus flufenamic acid (FFA) were reduced in the TRPC6-mut cells. Oscillations generated by hyperforin and FFA treatment were normalized to the fluorescence of the resting level (F_0), synchronized and averaged. (**b**) The average peak of Ca^{2+} influx in the 100 cells analyzed was reduced by 30% in the TRPC6-mut neural progenitor cells (NPCs) compared with the control sample when the cells were stimulated with hyperforin and FFA ($n = 3$; $P < 0.001$; analysis of variance (ANOVA)). (**c**) Representative western blot of neurons derived from a clone of a control and a TRPC6-mut induced pluripotent stem cell (iPSC) line treated or not treated with insulin-like growth factor-1 (IGF-1). (**d**) TRPC6-mut neurons displayed low levels of TRPC6 and synaptic proteins Psd-95, and synapsin I. IGF-1 treatment significantly increased the protein levels of TRPC6, Psd-95 and synapsin I in TRPC6-mut neurons ($n = 3$, $P < 0.01$; *t*-test). (**e**) Bar graphs showing that the total length (microns) and (**f**) number of vertices (neuronal branch points) of TRPC6-mut neurons is reduced compared with the controls. Treatment with hyperforin or restoring TRPC6 expression levels rescued these defects ($P < 0.01$; ANOVA). (**g**) Representative images of TRPC6-mut and control neurons before and after neuronal tracing. The neuronal morphology was visualized using the syn::enhanced green fluorescent protein (EGFP) lentiviral vector. Bar = 50 μm. (**h**) Bar graphs showing that the spine density in TRPC6-mut neurons was reduced compared with the controls and could be rescued after hyperforin treatment or restoring TRPC6 expression levels ($P < 0.01$; ANOVA). (**i**) A specific short-hairpin RNA (shRNA) against *TRPC6* (shTRPC6) was used to confirm that the phenotype was caused by loss of *TRPC6* function ($P < 0.01$; ANOVA). (**j**) Representative images of neuronal spines in control and TRPC6-mut neurons. (**k**) The bar graphs show that the number of glutamate vesicles in TRPC6-mut neurons was significantly reduced compared with the controls. IGF-1 and hyperforin treatment for 2 weeks increased the number of VGLUT1 puncta in TRPC6-mut neurons ($P < 0.01$; ANOVA). (**l**) Representative images of neurons stained for vesicular glutamate transporter-1 (VGLUT1) and microtubule-associated protein 2 (MAP2). (**m**) Control neurons expressing an shRNA against *TRPC6* (shTRPC6) exhibited reduced numbers of VGLUT1 puncta compared with the neurons expressing a scrambled shRNA (shScramble). (**n**) Representative image of a control neuron expressing an shRNA against *TRPC6*. Bar = 5 μm. (**o**) The bar graphs show the number of synaptic puncta, as measured by synapsin I staining. Synaptic puncta counts in TRPC6-mut neurons were reduced compared with the controls. TRPC6-complementary DNA (cDNA) treatment of TRPC6-mut neurons was sufficient to increase synapses to control levels ($P < 0.01$; $n = 20$; ANOVA). (**p**) Representative image of TRPC6-mut neurons with empty vector and with vector expressing wild-type TRPC6 stained for MAP2 and synapsin I. Bar = 5 μm. (**q**) The whole-cell Na^+ current of TRPC6-mut neurons was significantly less than that of the control ($P < 0.01$; ANOVA). (**r**) The Na^+ current density of TRPC6-mut neurons was also significantly less than that of the control ($P < 0.01$; ANOVA). (**s**) TRPC6 protein levels were reduced in neurons derived from an RTT iPSC clone expressing a non-functional version of MeCP2 compared with an isogenic control expressing the functional *MECP2* gene. (**t**) Recruitment of MeCP2 on the TRPC6 promoter region by ChIP. Extracts of formaldehyde-fixed neurons were precipitated with a MeCP2 antibody and analyzed by quantitative PCR (qPCR) using two distinct primers for the *TRPC6* promoter. The data show enrichment over the immunoglobulin G (IgG) control precipitation. The primers for the brain-derived neurotrophic factor (BDNF) promoter were used as controls. The numbers of neurons analyzed (*n*) are shown within the bars in graphs. The error bars in all panels show the s.e.m. For the iPSC clones used in each experiment, refer to Supplementary Table S4. *$P < 0.05$; **$P < 0.01$; ***$P < 0.001$.

focusing on *TRPC6* to conduct a single gene case–control association study. We screened targeted high-throughput sequencing data from all coding exons and splice sites of *TRPC6* in 1041 ASD cases from the SSC[26] and 942 ancestrally matched controls from the NINDS Neurologically Normal Caucasian Control Panel (http://ccr.coriell.org/Sections/Collections/NINDS/). A summary of

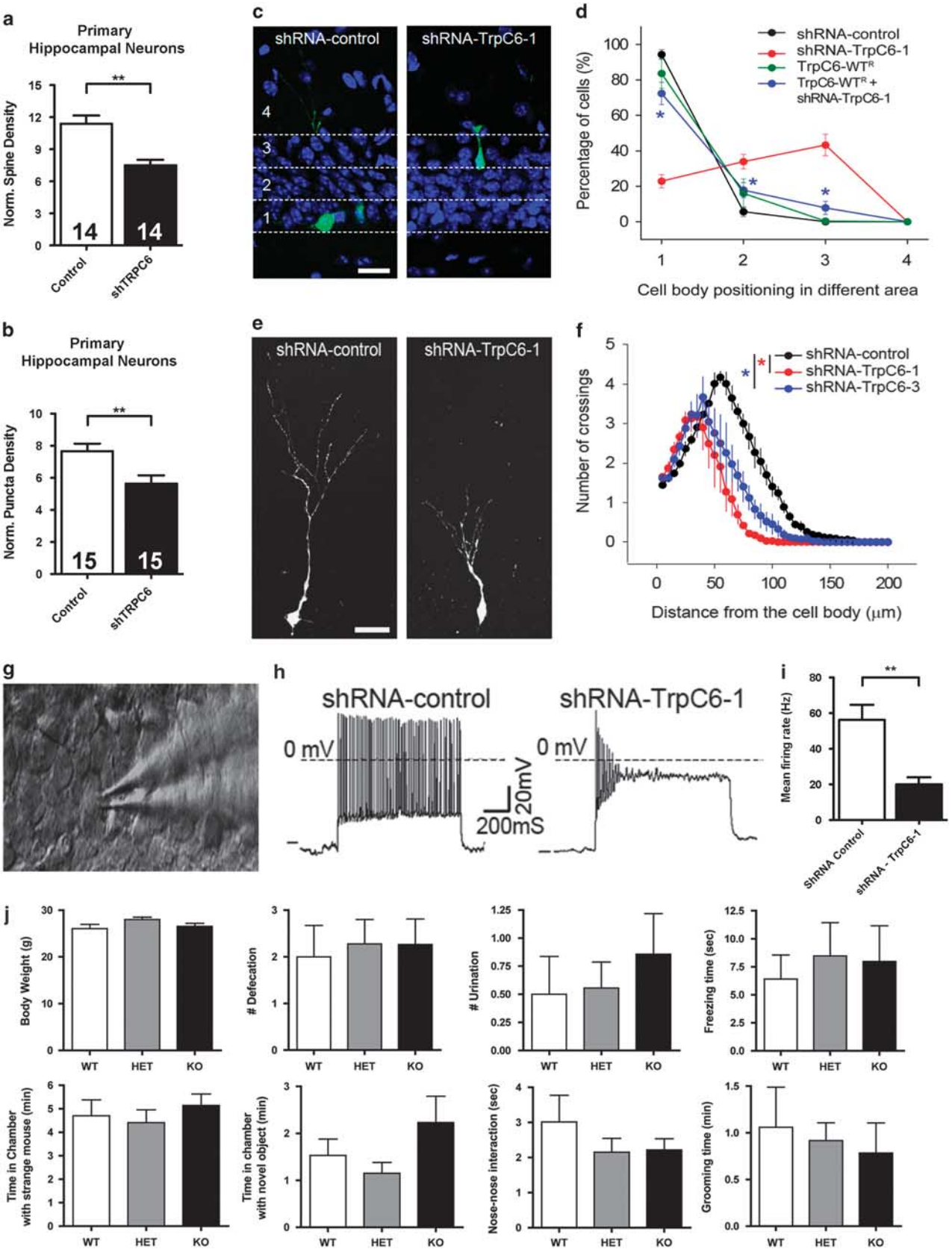

Figure 5. See for caption on page 1362.

the quality control metrics of the high-throughput sequencing is presented in Supplementary Table S7. We focused on novel splice sites, missense and nonsense mutations that were observed only once across all of our cohorts and not present in the dbSNP137 and 6503 exomes available from the Exome Variant Server (v.0.0.15). We reasoned that these variants were most likely to be deleterious and subject to purifying selection. Supplementary Table S8 lists all such variants in *TRPC6*. We observed significantly more novel nonsynonymous singleton mutations in cases compared with the controls (10/1041 cases versus 1/942 controls; $P = 0.013$, odds ratio = 9.127, 95% confidence interval = 1.211–191.027, Fisher's exact test, two-tailed). To confirm the low mutation rate observed in this control sample, we examined the whole-exome-sequencing data from an in-house database and identified an additional 1930 NE controls who clustered tightly with the HapMap CEU cohort. We evaluated the coding exons and splice sites of *TRPC6* and, to maximize sensitivity, did not set a minimum read threshold to identify all novel nonsynonymous singleton variants, which are listed in Supplementary Table S8. An omnibus analysis revealed an even more significant over-representation of such variants in cases (10/1041 cases versus 4/2872 controls; $P = 0.001$, odds ratio = 6.954, 95% confidence interval = 2.008–26.321, Fisher's exact test, two-tailed). As our results indicate that *TRPC6* disruption leads to haploinsufficiency of the corresponding protein, two of the case variants are particularly noteworthy: M1K, which disrupts the start codon; and Q3X, which is a very early premature stop codon. Unfortunately, live cells from these individuals were not available for follow-up functional studies. No *TRPC6* mutations affecting the start codon or nonsense mutations were identified in a total of 7445 controls: 942 NINDS neurologically normal Europeans and 6503 exomes from the Exome Variant Server (4300 European-American and 2203 African-American). Segregation analysis of the case variants revealed that each was inherited from an apparently unaffected parent, suggesting that these variants are incompletely penetrant, as has been previously observed for a wide range of ASD mutations such as Shank3.[62] Thus, although these genetic variations cannot be considered as causal mutations, they may represent risk factors for ASD. No *TRPC6* CNVs have been described in ASD (http://projects.tcag.ca/autism_500k).

DISCUSSION

A rapidly increasing number of ASD risk regions are being identified, and there is now considerable effort focused on moving from gene discovery to understanding the biological influences of these various mutations.[2–4,63–65] The development of relevant human-derived cellular models to study ASDs represents a complementary strategy to link genetic alterations to molecular mechanisms and complex behavioral and cognitive phenotypes.[66] Here, we identified the disruption of the *TRPC6* gene by a balanced *de novo* translocation in a non-syndromic ASD individual. *TRPC6* is involved in the regulation of axonal guidance, dendritic spine growth and excitatory synapse formation,[8,9,35] processes that have been consistently implicated in ASD etiology.[67–70] To explore if *TRPC6* disruption could result in such neuronal alterations, we made use of several different cellular models.

Global transcriptional studies of DPCs derived from the ASD individual and expression analysis upon activation of TRPC6 in DPCs and NPCs suggested that *TRPC6* signaling regulates the transcription of genes involved in neuronal adhesion, neurite growth and axonal guidance. The abnormal dysregulation found in the ASD individual may be triggered, at least for some genes, by reduced levels of phosphorylated CREB, a transcription factor activated by TRPC6 signaling.[8] CREB controls a complex regulatory network involved in memory formation, neuronal development and plasticity in the mammalian brain, processes that are compromised in ASD.[71–73]

Reprogramming the DPCs from the ASD individual to a pluripotent state allowed us to explore the functional consequences of *TRPC6* disruption in human neuronal cells. Ca^{2+} influx was aberrant in NPCs derived from the ASD individual, suggesting that Ca^{2+} signaling-dependent mechanisms were compromised in these cells. Ca^{2+} signaling pathways have previously been implicated in ASD etiology; mutations in different voltage-gated Ca^{+2} channels and Ca^{+2}-regulated signaling molecules have been

Figure 5. TRPC6 regulates the neural development of adult-born neurons in the dentate gyrus of the hippocampus. (**a**) Mouse primary hippocampal neurons revealed reduced spine density in neurons treated with short-hairpin RNA (shRNA) targeting TRPC6 compared with neurons treated with shRNA scramble control ($P < 0.01$; $n = 14$; *t*-test). (**b**) Mouse primary hippocampal neurons demonstrated reduced synaptic puncta numbers in neurons treated with shRNA targeting TRPC6 compared with neurons treated with shRNA scramble control ($P < 0.01$; $n = 15$; *t*-test). Synaptic puncta were labeled using synapsin I antibodies and counted along microtubule-associated protein 2^+ ($MAP2^+$) neuronal dendrites. (**c**) Representative confocal images of neurons expressing shRNA-control and shRNA-TRPC6-1 at 28 days postretroviral injection (d.p.i.). Green, green fluorescent protein (GFP); blue, 4,6-diamidino-2-phenylindole (DAPI). Bar = 50 μm. Also shown are the divided areas of the dentate gyrus: 1, inner granule cell layer; 2, middle granule cell layer; 3, upper granule cell layer; and 4, molecular layer. (**d**) Summary of cell body localization of GFP^+ newborn neurons under different experimental conditions at 28 d.p.i. The cell migration phenotype was rescued by expression of TRPC6-WT^R at 14 d.p.i. Retroviruses co-expressing GFP and TrpC6-WT^R were co-injected with retroviruses co-expressing dsRed and shRNA-TRPC6-1 into the adult mouse dentate gyri. The cell body localization of the GFP^+, $DsRed^+$ and GFP^+DsRed^+ neurons are quantified. The values represent the mean ± s.e.m. ($n = 3$; $P < 0.01$; analysis of variance (ANOVA)). (**e**) A three-dimensional confocal reconstruction of dendritic trees of GFP^+ dentate granule cells expressing shRNA-control or shRNA-TRPC6-1 at 14 d.p.i. Scale bar, 20 μm. (**f**) Sholl analysis of the dendritic complexity of GFP^+ neurons at 14 d.p.i. Number of crossings refers to the number of dendrites intersecting concentric circles spaced 10 μm apart starting from the cell body. The error bars in all panels show the s.e.m. ($n = 3$; $P < 0.05$; ANOVA). (**g**) A sample DIC image of a newborn neuron patched in whole-cell configuration in an acute slice of the hippocampus. (**h**) The firing rate of repetitive action potentials of GFP^+ neurons under current clamp in response to 1-s current injection steps at 21 d.p.i. Shown on the left is a sample trace of a GFP^+ neuron expressing shRNA-control; a GFP^+ neuron expressing shRNA-TRPC6#-1 is shown on the right. (**i**) Summary of the mean firing rate of newborn neurons. The values represent the mean ± s.d. ($n = 3$; $P < 0.01$; ANOVA). A minimum of 10 GFP^+ cells was randomly picked from each animal, and at least three animals (*n*) under each experimental condition were used. (**j**) Behavioral analysis of *Trpc6* knockout (KO) and heterozygote (HET) mice. The mean body weight and defecation and urination episodes during the test revealed no physiological differences between the wild-type (WT), HET and KO *Trpc6* animals. Evaluation of time spent in freezing behavior and in grooming behavior revealed no significant differences between the groups. Social interaction was assessed by evaluating the time spent with a novel object or in nose-to-nose contact with a strange animal. Adult mice (6–8 weeks old, male) in a C57BL/6 background were used for the study. At least 12 animals per group were utilized in biological replicates. The experimenter was blind to the genotypes. The data were analyzed using non-parametric Kruskal–Wallis ANOVA. The error bars in all panels show the s.e.m. All procedures followed institutional guidelines. *$P < 0.05$; **$P < 0.01$.

identified in ASD individuals.[74–77] This result, combined with the measured protein levels, reveals that disruption of *TRPC6* leads to a functionally relevant haploinsufficiency, making the existence of a novel disease-relevant protein resulting from a *TRPC6* and *VPRBP* combination unlikely.

In human neurons, *TRPC6* haploinsufficiency causes other functional and morphological alterations that reflect defects in axonal and dendritic growth, such as shortening of neurites, a decrease in arborization and a reduction in dendritic spine density. Alterations in these phenotypes were already been described for postmortem or iPSC-derived ASD neurons.[78,79] Analysis of neurons derived from the ASD individual's iPSCs also revealed a reduction of VGLUT1 puncta density, in agreement with previous work demonstrating that *TRPC6* expression levels can modulate glutamatergic synapse formation in rat neurons.[9] Alterations in glutamatergic neurotransmission have been identified in individuals with syndromic forms of ASD: dysregulation of the metabotropic glutamate receptor 1/5 pathway has been well documented in Fragile-X syndrome, and neurons derived from RTT patient iPSCs also present a reduction in the number of VGLUT1 puncta.[6,80,81] In addition, a reduction in glutamatergic transmission was observed in Shank3 HET mice, an ASD mouse model.[82] Finally, Na^+ currents were also decreased in ASD individual's neurons. This result is in agreement with previous findings that demonstrate that TRPC6 channels participate in Na^+ cell entry.[38] Decreased Na^+ current densities have previously been reported in other ASD models.[83]

Owing to the high degree of locus heterogeneity, it is challenging to identify additional individuals carrying similar rare variants in the ASD population. Therefore, we used complementary functional assays such as loss-of-function experiments and mouse models to validate the observation that reduction in *TRPC6* expression levels lead to abnormal neuronal phenotypes and is important for neuronal homeostasis. Moreover, we have demonstrated that several of the phenotypic alterations seen in the TRPC6-mut neurons could be rescued by both using hyperforin, which activates the channel, and expressing WT *TRPC6*. These *TRPC6* loss-of-function and complementation assays underscore its importance for neuronal homeostasis. Based on the results obtained from our different cellular models, this is likely due to *TRPC6* influence on Ca^{2+}-signaling-dependent mechanisms and neuronal transcriptional regulation. The common altered neuronal phenotypes shared by the TRPC6-mut individual and RTT patients support the idea that ASD caused by different genetic mechanisms affect common pathways. Indeed, our data suggest that MeCP2 may act upstream of *TRPC6*, regulating its expression. Previous mouse studies [53,54] suggested similar findings but failed to show a direct link between MeCP2 and the *TRPC6* promoter through ChIP assays, likely due to the poor conservation between the promoter regions in these two species. Additional studies using large samples of idiopathic ASD individuals will help address this hypothesis.

Our findings also provide insights supporting the testing of novel drugs in ASD such as hyperforin, a drug that specifically activates TRPC6,[38,84] or IGF-1, which may increase not only TRPC6 protein levels but also other synaptic components. Therefore, individuals with alterations in this pathway may benefit from these drugs. These defects could also be rescued by activating the AKT/mTOR pathway using IGF-1. The TRPC6 KO mice exhibit reduced exploratory interest, a typical ASD-like behavior, but no impaired social interaction or repetitive movements. The lack of some ASD-like behaviors in mouse models is common and can be attributed to the inherent differences between human and mouse genetic backgrounds and neural circuits.[85–88] Alternatively, other genetic alterations may be required to develop the full autistic phenotype in this mouse model. Accumulating evidence favors the multiple-hit model in a significant proportion of ASD individuals, as well as in the case of the ASD individual described here.[89–92] In fact, although our functional data demonstrate that *TRPC6* has a crucial role in synaptogenesis and is involved in pathways previously associated with ASD, our mutation screening data suggest rare *TRPC6* variants may have a more moderate contribution to the disease. Our sequencing findings revealed *TRPC6* loss-of-function mutations in two ASD families with incomplete penetrance of the phenotype, supporting the multi-hit hypothesis for ASD. Indeed, the individual studied here also presents other rare genetic variants, such as in the ASD associated gene *PDE4A* or even *VPRBP*, which may contribute to his phenotype. However, this does not diminish the impact of TRPC6 to the phenotype, as our experiments using hyperforin or *TRPC6* complementation rescued the observed cellular alterations. This suggests that although other genetic alterations present in the individual may augment the observed phenotypes, *TRPC6* disruption is the predominant contributor to the abnormal neuronal function in this ASD individual.

Thus, our results suggest *TRPC6* as a novel predisposing gene for ASD that likely acts in combination with other genetic variants to contribute to autistic phenotypes. Our work demonstrates that individual-specific iPSC-derived neurons can be used to correlate novel variants in ASD individuals to the etiology of these highly complex disorders.

CONFLICT OF INTEREST

The authors declare no conflict of interest.

ACKNOWLEDGMENTS

The work was supported by grants from the California Institute for Regenerative Medicine (CIRM) TR2-01814, the National Institutes of Health through the NIH Director's New Innovator Award Program (1-DP2-OD006495-01), A NARSAD Independent Investigator Grant to ARM; a NIH predoctoral training grant T32 GM008666 to AA; Fundação de Amparo a Pesquisa do Estado de São Paulo (FAPESP), Conselho Nacional de Desenvolvimento Científico e Tecnológico (CNPq), and by NIH (NS047344) and SAFRI to HS; NIH (NS048271, HD069184), NARSAD and MSCRF to GL; NIH (K08MH087639) to ARG; and NIH (RC2MH089956) to MWS. We would like to thank the ASD individuals and their families, Daniela Franco Bueno and Gerson Shigeru Kobayashi for the DPC control samples, Kristin Rose for technical support, and Dr Willmar Schwabe, GmbH & Co, Karlsruhe, Germany, for providing hyperforin.

REFERENCES

1 State MW, Levitt P. The conundrums of understanding genetic risks for autism spectrum disorders. *Nat Neurosci* 2011; **14**: 1499–1506.
2 Sanders SJ, Ercan-Sencicek AG, Hus V, Luo R, Murtha MT, Moreno-De-Luca D *et al.* Multiple recurrent de novo CNVs, including duplications of the 7q11.23 Williams syndrome region, are strongly associated with autism. *Neuron* 2011; **70**: 863–885.
3 Sanders SJ, Murtha MT, Gupta AR, Murdoch JD, Raubeson MJ, Willsey AJ *et al.* De novo mutations revealed by whole-exome sequencing are strongly associated with autism. *Nature* 2012; **485**: 237–241.
4 Neale BM, Kou Y, Liu L, Ma'ayan A, Samocha KE, Sabo A *et al.* Patterns and rates of exonic de novo mutations in autism spectrum disorders. *Nature* 2012; **485**: 242–245.
5 Takahashi K, Tanabe K, Ohnuki M, Narita M, Ichisaka T, Tomoda K *et al.* Induction of pluripotent stem cells from adult human fibroblasts by defined factors. *Cell* 2007; **131**: 861–872.
6 Marchetto MC, Carromeu C, Acab A, Yu D, Yeo GW, Mu Y *et al.* A model for neural development and treatment of Rett syndrome using human induced pluripotent stem cells. *Cell* 2010; **143**: 527–539.
7 Muotri AR, Marchetto MC, Coufal NG, Oefner R, Yeo G, Nakashima K *et al.* L1 retrotransposition in neurons is modulated by MeCP2. *Nature* 2010; **468**: 443–446.
8 Tai Y, Feng S, Ge R, Du W, Zhang X, He Z *et al.* TRPC6 channels promote dendritic growth via the CaMKIV-CREB pathway. *J Cell Sci* 2008; **121**: 2301–2307.
9 Zhou J, Du W, Zhou K, Tai Y, Yao H, Jia Y *et al.* Critical role of TRPC6 channels in the formation of excitatory synapses. *Nat Neurosci* 2008; **11**: 741–743.
10 Wang K, Li M, Hadley D, Liu R, Glessner J, Grant SF *et al.* PennCNV: an integrated hidden Markov model designed for high-resolution copy number variation detection in whole-genome SNP genotyping data. *Genome Res* 2007; **17**: 1665–1674.

11 Colella S, Yau C, Taylor JM, Mirza G, Butler H, Clouston P *et al.* QuantiSNP: an Objective Bayes Hidden-Markov Model to detect and accurately map copy number variation using SNP genotyping data. *Nucleic Acids Res* 2007; **35**: 2013–2025.
12 Lichter P, Tang CJ, Call K, Hermanson G, Evans GA, Housman D *et al.* High-resolution mapping of human chromosome 11 by in situ hybridization with cosmid clones. *Science* 1990; **247**: 64–69.
13 Beltrao-Braga PI, Pignatari GC, Maiorka PC, Oliveira NA, Lizier NF, Wenceslau CV *et al.* Feeder-free derivation of induced pluripotent stem cells from human immature dental pulp stem cells. *Cell Transplant* 2011; **20**: 1707–1719.
14 Irizarry RA, Hobbs B, Collin F, Beazer-Barclay YD, Antonellis KJ, Scherf U *et al.* Exploration, normalization, and summaries of high density oligonucleotide array probe level data. *Biostatistics* 2003; **4**: 249–264.
15 Tusher VG, Tibshirani R, Chu G. Significance analysis of microarrays applied to the ionizing radiation response. *Proc Natl Acad Sci USA* 2001; **98**: 5116–5121.
16 Breitling R, Armengaud P, Amtmann A, Herzyk P. Rank products: a simple, yet powerful, new method to detect differentially regulated genes in replicated microarray experiments. *FEBS Lett* 2004; **573**: 83–92.
17 Zhang X, Odom DT, Koo SH, Conkright MD, Canettieri G, Best J *et al.* Genome-wide analysis of cAMP-response element binding protein occupancy, phosphorylation, and target gene activation in human tissues. *Proc Natl Acad Sci USA* 2005; **102**: 4459–4464.
18 Livak KJ, Schmittgen TD. Analysis of relative gene expression data using real-time quantitative PCR and the 2(-Delta Delta C(T)) Method. *Methods* 2001; **25**: 402–408.
19 Vandesompele J, De Preter K, Pattyn F, Poppe B, Van Roy N, De Paepe A *et al.* Accurate normalization of real-time quantitative RT-PCR data by geometric averaging of multiple internal control genes. *Genome Biol* 2002; **3**: 0034.1–0034.11.
20 Muotri AR, Chu VT, Marchetto MC, Deng W, Moran JV, Gage FH. Somatic mosaicism in neuronal precursor cells mediated by L1 retrotransposition. *Nature* 2005; **435**: 903–910.
21 Martinowich K, Hattori D, Wu H, Fouse S, He F, Hu Y *et al.* DNA methylation-related chromatin remodeling in activity-dependent BDNF gene regulation. *Science* 2003; **302**: 890–893.
22 Kim JY, Duan X, Liu CY, Jang MH, Guo JU, Pow-anpongkul N *et al.* DISC1 regulates new neuron development in the adult brain via modulation of AKT-mTOR signaling through KIAA1212. *Neuron* 2009; **63**: 761–773.
23 Duan X, Chang JH, Ge S, Faulkner RL, Kim JY, Kitabatake Y *et al.* Disrupted-in-schizophrenia 1 regulates integration of newly generated neurons in the adult brain. *Cell* 2007; **130**: 1146–1158.
24 Kang E, Burdick KE, Kim JY, Duan X, Guo JU, Sailor KA *et al.* Interaction between FEZ1 and DISC1 in regulation of neuronal development and risk for schizophrenia. *Neuron* 2011; **72**: 559–571.
25 Ge S, Goh EL, Sailor KA, Kitabatake Y, Ming GL, Song H. GABA regulates synaptic integration of newly generated neurons in the adult brain. *Nature* 2006; **439**: 589–593.
26 Fischbach GD, Lord C. The Simons simplex collection: a resource for identification of autism genetic risk factors. *Neuron* 2010; **68**: 192–195.
27 Xu LM, Li JR, Huang Y, Zhao M, Tang X, Wei L. AutismKB: an evidence-based knowledgebase of autism genetics. *Nucleic Acids Res* 2012; **40**: D1016–D1022.
28 Braun NN, Reutiman TJ, Lee S, Folsom TD, Fatemi SH. Expression of phosphodiesterase 4 is altered in the brains of subjects with autism. *Neuroreport* 2007; **18**: 1841–1844.
29 Gronthos S, Brahim J, Li W, Fisher LW, Cherman N, Boyde A *et al.* Stem cell properties of human dental pulp stem cells. *J Dent Res* 2002; **81**: 531–535.
30 Miura M, Gronthos S, Zhao M, Lu B, Fisher LW, Robey PG *et al.* SHED: stem cells from human exfoliated deciduous teeth. *Proc Natl Acad Sci USA* 2003; **100**: 5807–5812.
31 d'Aquino R, De Rosa A, Laino G, Caruso F, Guida L, Rullo R *et al.* Human dental pulp stem cells: from biology to clinical applications. *J Exp Zool B Mol Dev Evol* 2009; **312B**: 408–415.
32 Griesi-Oliveira K, Sunaga DY, Alvizi L, Vadasz E, Passos-Bueno MR. Stem cells as a good tool to investigate dysregulated biological systems in autism spectrum disorders. *Autism Res* 2013; **6**: 354–361.
33 Kashiwa A, Yoshida H, Lee S, Paladino T, Liu Y, Chen Q *et al.* Isolation and characterization of novel presenilin binding protein. *J Neurochem* 2000; **75**: 109–116.
34 Tai Y, Feng S, Du W, Wang Y. Functional roles of TRPC channels in the developing brain. *Pflugers Arch* 2009; **458**: 283–289.
35 Li Y, Jia YC, Cui K, Li N, Zheng ZY, Wang YZ *et al.* Essential role of TRPC channels in the guidance of nerve growth cones by brain-derived neurotrophic factor. *Nature* 2005; **434**: 894–898.
36 Jia Y, Zhou J, Tai Y, Wang Y. TRPC channels promote cerebellar granule neuron survival. *Nat Neurosci* 2007; **10**: 559–567.
37 McCall CM, Miliani de Marval PL, Chastain PD 2nd, Jackson SC, He YJ, Kotake Y *et al.* Human immunodeficiency virus type 1 Vpr-binding protein VprBP, a WD40 protein associated with the DDB1-CUL4 E3 ubiquitin ligase, is essential for DNA replication and embryonic development. *Mol Cell Biol* 2008; **28**: 5621–5633.
38 Leuner K, Kazanski V, Muller M, Essin K, Henke B, Gollasch M *et al.* Hyperforin--a key constituent of St. John's wort specifically activates TRPC6 channels. *Faseb J* 2007; **21**: 4101–4111.
39 Muller M, Essin K, Hill K, Beschmann H, Rubant S, Schempp CM *et al.* Specific TRPC6 channel activation, a novel approach to stimulate keratinocyte differentiation. *J Biol Chem* 2008; **283**: 33942–33954.
40 Leuner K, Heiser JH, Derksen S, Mladenov MI, Fehske CJ, Schubert R *et al.* Simple 2,4-diacylphloroglucinols as classic transient receptor potential-6 activators--identification of a novel pharmacophore. *Mol Pharmacol* 2010; **77**: 368–377.
41 Chen J, Lin M, Foxe JJ, Pedrosa E, Hrabovsky A, Carroll R *et al.* Transcriptome comparison of human neurons generated using induced pluripotent stem cells derived from dental pulp and skin fibroblasts. *PLoS One* 2013; **8**: e75682.
42 Fiorio Pla A, Maric D, Brazer SC, Giacobini P, Liu X, Chang YH *et al.* Canonical transient receptor potential 1 plays a role in basic fibroblast growth factor (bFGF)/FGF receptor-1-induced Ca2+ entry and embryonic rat neural stem cell proliferation. *J Neurosci* 2005; **25**: 2687–2701.
43 Cukier HN, Lee JM, Ma D, Young JI, Mayo V, Butler BL *et al.* The expanding role of MBD genes in autism: identification of a MECP2 duplication and novel alterations in MBD5, MBD6, and SETDB1. *Autism Res* 2012; **5**: 385–397.
44 Cukier HN, Rabionet R, Konidari I, Rayner-Evans MY, Baltos ML, Wright HH *et al.* Novel variants identified in methyl-CpG-binding domain genes in autistic individuals. *Neurogenetics* 2010; **11**: 291–303.
45 Kuwano Y, Kamio Y, Kawai T, Katsuura S, Inada N, Takaki A *et al.* Autism-associated gene expression in peripheral leucocytes commonly observed between subjects with autism and healthy women having autistic children. *PLoS One* 2011; **6**: e24723.
46 Campos M Jr., Pestana CP, dos Santos AV, Ponchel F, Churchman S, Abdalla-Carvalho CB *et al.* A MECP2 missense mutation within the MBD domain in a Brazilian male with autistic disorder. *Brain Dev* 2011; **33**: 807–809.
47 Piton A, Gauthier J, Hamdan FF, Lafreniere RG, Yang Y, Henrion E *et al.* Systematic resequencing of X-chromosome synaptic genes in autism spectrum disorder and schizophrenia. *Mol Psychiatry* 2011; **16**: 867–880.
48 Dotti MT, Orrico A, De Stefano N, Battisti C, Sicurelli F, Severi S *et al.* A Rett syndrome MECP2 mutation that causes mental retardation in men. *Neurology* 2002; **58**: 226–230.
49 Lam CW, Yeung WL, Ko CH, Poon PM, Tong SF, Chan KY *et al.* Spectrum of mutations in the MECP2 gene in patients with infantile autism and Rett syndrome. *J Med Genet* 2000; **37**: E41.
50 Carney RM, Wolpert CM, Ravan SA, Shahbazian M, Ashley-Koch A, Cuccaro ML *et al.* Identification of MeCP2 mutations in a series of females with autistic disorder. *Pediatr Neurol* 2003; **28**: 205–211.
51 Nagarajan RP, Hogart AR, Gwye Y, Martin MR, LaSalle JM. Reduced MeCP2 expression is frequent in autism frontal cortex and correlates with aberrant MECP2 promoter methylation. *Epigenetics* 2006; **1**: e1–11.
52 Samaco RC, Nagarajan RP, Braunschweig D, LaSalle JM. Multiple pathways regulate MeCP2 expression in normal brain development and exhibit defects in autism-spectrum disorders. *Hum Mol Genet* 2004; **13**: 629–639.
53 Chahrour M, Jung SY, Shaw C, Zhou X, Wong ST, Qin J *et al.* MeCP2, a key contributor to neurological disease, activates and represses transcription. *Science* 2008; **320**: 1224–1229.
54 Li W, Calfa G, Larimore J, Pozzo-Miller L. Activity-dependent BDNF release and TRPC signaling is impaired in hippocampal neurons of Mecp2 mutant mice. *Proc Natl Acad Sci USA* 2012; **109**: 17087–17092.
55 Tropea D, Giacometti E, Wilson NR, Beard C, McCurry C, Fu DD *et al.* Partial reversal of Rett Syndrome-like symptoms in MeCP2 mutant mice. *Proc Natl Acad Sci USA* 2009; **106**: 2029–2034.
56 Khwaja OS, Ho E, Barnes KV, O'Leary HM, Pereira LM, Finkelstein Y *et al.* Safety, pharmacokinetics, and preliminary assessment of efficacy of mecasermin (recombinant human IGF-1) for the treatment of Rett syndrome. *Proc Natl Acad Sci USA* 2014; **111**: 4596–4601.
57 Leuner K, Li W, Amaral MD, Rudolph S, Calfa G, Schuwald AM *et al.* Hyperforin modulates dendritic spine morphology in hippocampal pyramidal neurons by activating Ca(2+) -permeable TRPC6 channels. *Hippocampus* 2012; **23**: 40–52.
58 Ming GL, Song H. Adult neurogenesis in the mammalian brain: significant answers and significant questions. *Neuron* 2011; **70**: 687–702.
59 Dietrich A, Mederos YSM, Gollasch M, Gross V, Storch U, Dubrovska G *et al.* Increased vascular smooth muscle contractility in TRPC6-/- mice. *Mol Cell Biol* 2005; **25**: 6980–6989.
60 Beis D, Schwarting RK, Dietrich A. Evidence for a supportive role of classical transient receptor potential 6 (TRPC6) in the exploration behavior of mice. *Physiol Behav* **102**: 245–250.
61 Pierce K, Courchesne E. Evidence for a cerebellar role in reduced exploration and stereotyped behavior in autism. *Biol Psychiatry* 2001; **49**: 655–664.

62 Durand CM, Betancur C, Boeckers TM, Bockmann J, Chaste P, Fauchereau F *et al.* Mutations in the gene encoding the synaptic scaffolding protein SHANK3 are associated with autism spectrum disorders. *Nat Genet* 2007; **39**: 25–27.
63 Iossifov I, Ronemus M, Levy D, Wang Z, Hakker I, Rosenbaum J *et al. De novo* gene disruptions in children on the autistic spectrum. *Neuron* 2012; **74**: 285–299.
64 O'Roak BJ, Vives L, Girirajan S, Karakoc E, Krumm N, Coe BP *et al.* Sporadic autism exomes reveal a highly interconnected protein network of *de novo* mutations. *Nature* 2012; **485**: 246–250.
65 Talkowski ME, Rosenfeld JA, Blumenthal I, Pillalamarri V, Chiang C, Heilbut A *et al.* Sequencing chromosomal abnormalities reveals neurodevelopmental loci that confer risk across diagnostic boundaries. *Cell* 2012; **149**: 525–537.
66 Chailangkarn T, Acab A, Muotri AR. Modeling neurodevelopmental disorders using human neurons. *Curr Opin Neurobiol* 2012; **22**: 785–790.
67 Sbacchi S, Acquadro F, Calo I, Cali F, Romano V. Functional annotation of genes overlapping copy number variants in autistic patients: focus on axon pathfinding. *Curr Genomics* 2010; **11**: 136–145.
68 Voineagu I, Wang X, Johnston P, Lowe JK, Tian Y, Horvath S *et al.* Transcriptomic analysis of autistic brain reveals convergent molecular pathology. *Nature* 2011; **474**: 380–384.
69 Cruz-Martin A, Crespo M, Portera-Cailliau C. Delayed stabilization of dendritic spines in fragile X mice. *J Neurosci* 2010; **30**: 7793–7803.
70 Chapleau CA, Larimore JL, Theibert A, Pozzo-Miller L. Modulation of dendritic spine development and plasticity by BDNF and vesicular trafficking: fundamental roles in neurodevelopmental disorders associated with mental retardation and autism. *J Neurodev Disord* 2009; **1**: 185–196.
71 Lonze BE, Riccio A, Cohen S, Ginty DD. Apoptosis, axonal growth defects, and degeneration of peripheral neurons in mice lacking CREB. *Neuron* 2002; **34**: 371–385.
72 Balschun D, Wolfer DP, Gass P, Mantamadiotis T, Welzl H, Schutz G *et al.* Does cAMP response element-binding protein have a pivotal role in hippocampal synaptic plasticity and hippocampus-dependent memory? *J Neurosci* 2003; **23**: 6304–6314.
73 Dworkin S, Mantamadiotis T. Targeting CREB signalling in neurogenesis. *Expert Opin Ther Targets* 2010; **14**: 869–879.
74 Hemara-Wahanui A, Berjukow S, Hope CI, Dearden PK, Wu SB, Wilson-Wheeler J *et al.* A CACNA1F mutation identified in an X-linked retinal disorder shifts the voltage dependence of Cav1.4 channel activation. *Proc Natl Acad Sci USA* 2005; **102**: 7553–7558.
75 Krey JF, Dolmetsch RE. Molecular mechanisms of autism: a possible role for Ca2+ signaling. *Curr Opin Neurobiol* 2007; **17**: 112–119.
76 Splawski I, Timothy KW, Sharpe LM, Decher N, Kumar P, Bloise R *et al.* Ca(V)1.2 calcium channel dysfunction causes a multisystem disorder including arrhythmia and autism. *Cell* 2004; **119**: 19–31.
77 Splawski I, Yoo DS, Stotz SC, Cherry A, Clapham DE, Keating MT. CACNA1H mutations in autism spectrum disorders. *J Biol Chem* 2006; **281**: 22085–22091.
78 Belichenko PV, Oldfors A, Hagberg B, Dahlstrom A. Rett syndrome: 3-D confocal microscopy of cortical pyramidal dendrites and afferents. *Neuroreport* 1994; **5**: 1509–1513.
79 Marchetto MC, Brennand KJ, Boyer LF, Gage FH. Induced pluripotent stem cells (iPSCs) and neurological disease modeling: progress and promises. *Hum Mol Genet* 2011; **20**: R109–R115.
80 Hagerman R, Hoem G, Hagerman P. Fragile X and autism: Intertwined at the molecular level leading to targeted treatments. *Mol Autism* 2010; **1**: 12.
81 Bear MF, Huber KM, Warren ST. The mGluR theory of fragile X mental retardation. *Trends Neurosci* 2004; **27**: 370–377.
82 Bozdagi O, Sakurai T, Papapetrou D, Wang X, Dickstein DL, Takahashi N *et al.* Haploinsufficiency of the autism-associated Shank3 gene leads to deficits in synaptic function, social interaction, and social communication. *Mol Autism* 2010; **1**: 15.
83 Han S, Tai C, Westenbroek RE, Yu FH, Cheah CS, Potter GB *et al.* Autistic-like behaviour in Scn1a+/− mice and rescue by enhanced GABA-mediated neurotransmission. *Nature* 2012; **489**: 385–390.
84 Muller WE. Current St John's wort research from mode of action to clinical efficacy. *Pharmacol Res* 2003; **47**: 101–109.
85 Wohr M, Silverman JL, Scattoni ML, Turner SM, Harris MJ, Saxena R *et al.* Developmental delays and reduced pup ultrasonic vocalizations but normal sociability in mice lacking the postsynaptic cell adhesion protein neuroligin2. *Behav Brain Res* 2012; **251**: 50–64.
86 Silverman JL, Yang M, Lord C, Crawley JN. Behavioural phenotyping assays for mouse models of autism. *Nat Rev Neurosci* 2010; **11**: 490–502.
87 Xu JY, Xia QQ, Xia J. A review on the current neuroligin mouse models. *Sheng Li Xue Bao* 2012; **64**: 550–562.
88 Oddi D, Crusio WE, D'Amato FR, Pietropaolo S. Monogenic mouse models of social dysfunction: Implications for autism. *Behav Brain Res* 2013; **251**: 75–84.
89 Poot M, Beyer V, Schwaab I, Damatova N, Van't Slot R, Prothero J *et al.* Disruption of CNTNAP2 and additional structural genome changes in a boy with speech delay and autism spectrum disorder. *Neurogenetics* 2010; **11**: 81–89.
90 Poot M, van der Smagt JJ, Brilstra EH, Bourgeron T. Disentangling the myriad genomics of complex disorders, specifically focusing on autism, epilepsy, and schizophrenia. *Cytogenet Genome Res* 2011; **135**: 228–240.
91 Leblond CS, Heinrich J, Delorme R, Proepper C, Betancur C, Huguet G *et al.* Genetic and functional analyses of SHANK2 mutations suggest a multiple hit model of autism spectrum disorders. *PLoS Genet* 2012; **8**: e1002521.
92 Marshall CR, Noor A, Vincent JB, Lionel AC, Feuk L, Skaug J *et al.* Structural variation of chromosomes in autism spectrum disorder. *Am J Hum Genet* 2008; **82**: 477–488.

Supplementary Information accompanies the paper on the Molecular Psychiatry website (http://www.nature.com/mp)